An International Journal of Optimization and Control: Theories & Applications
ISSN: 2146-0957 eISSN: 2146-5703
Vol.16, No.3, pp.948-980 (2026)
https://doi.org/10.36922/IJOCTA025450195

RESEARCH ARTICLE

Complex variable neural network controller for port-Hamiltonian systems with non-holonomic constraints

Fernando Serrano[1], Saim Ahmed[2*], Ahmad Taher Azar[2,3], and Ahmed Redha Mahlous[2,3]

[1]Institute of Robotics and Industrial Informatics IRI-CSIC, Technical University of Catalonia, Carrer de Llorens i Artigas, 4, Les Corts, Barcelona, Spain
[2]Automated Systems and Computing Lab (ASCL), Prince Sultan University, Riyadh, Saudi Arabia
[3]College of Computer and Information Sciences, Prince Sultan University, Riyadh, Saudi Arabia
fernando.serrano@ieee.org; sahmed@psu.edu.sa; aazar@psu.edu.sa; armahlous@psu.edu.sa

ARTICLE INFO

Article History:
Received: November 5, 2025
Revised: February 24, 2026
Accepted: February 27, 2026
Published Online: April 30, 2026

Keywords:
Neural networks
Neural control
Port-Hamiltonian systems
Dirac structures
Nonlinear systems
Unmanned aerial vehicles

AMS Classification 2010:
26A33; 34A08; 35H15; 34K50
47H10; 60H10

ABSTRACT

This study presents a complex variable neural network (CVNN) controller designed for unmanned aerial vehicles (UAVs) using the port-Hamiltonian formulation with non-holonomic constraints. The approach begins by deriving the dynamic model of a quadrotor UAV in port-Hamiltonian form, where the Hamiltonian is constructed from the system's total kinetic and potential energies. Dirac structures are implemented to preserve the system's structural properties while incorporating non-holonomic constraints specifically in the attitude loop. The proposed control architecture decouples the attitude and position control loops, with each utilizing a CVNN controller designed through Lyapunov stability analysis. Theoretical proofs establish the stability of both control loops, while numerical simulations demonstrate the effectiveness of the proposed approach for trajectory tracking tasks. Comparative analysis against existing controllers shows superior performance in reducing root mean square errors while maintaining reasonable control effort. The results confirm that the CVNN controller effectively manages the UAV's dynamic behavior even with non-holonomic constraints limiting the vehicle's orientation range.

1. Introduction

Unmanned aerial vehicles (UAVs) have been increasingly studied, considering the vast amount of civil and military applications. Due to the increase in tasks and novel UAV, the design of appropriate and suitable control strategies is crucial for this kind of robotic system. The port-Hamiltonian formulation provides significant advantages for modeling UAV dynamics as it explicitly accounts for energy properties and structural characteristics of these systems. Neural control strategies have emerged as fundamental approaches for UAVs, particularly when considering real-time hardware implementation in experimental or practical settings. This introduction provides a survey of the literature on the following issues, such as the practical applications of UAV, the implementation of the Dirac structure, the port-Hamiltonian formulation of UAVs, the non-Holonomic formulations of UAVs' dynamic models, neural control, and complex variable neural controllers.

Civil and military applications of UAVs are diverse, with implementations in plague control, surveillance, and search and rescue, among others. For example, in Pu *et al.*,[1] UAV were used for the inspection of solar/wind energy resources. In Li *et al.*,[2] computer vision-based UAV are used for pest monitoring in forests. Tarpenning *et al.*[3] compared the performance of UAV for the surveillance of trash sites in which *Aedes*

*Corresponding Author

aegypti were found. Furthermore, Xu *et al.*[4] used UAVs for the inspection of aerial power lines. Van Haeften,[5] performed the phenotyping of agronomics traits with UAVs, while Li *et al.*[6] used UAVs for a prototype of a space–air–ground network.

Other advances in the implementation of UAV can be found in Liller *et al.*,[7] in which a battery-free and solar-powered fixed-wing unmanned aerial vehicle is presented. Han[8] performed aerial tracking using the whale optimization and gray wolf optimizer. Moreover, Liu *et al.*,[9] presented the implementation of adaptive particle swarm optimization for trajectory planning of UAV.

This study extends beyond UAVs to include a broader range of unmanned vehicles, such as unmanned submarine vehicles or marine vessels. For example, in Bouzid *et al.*,[10] the port-controlled representation of a unmanned aerial vehicle with flight constraint is obtained to derive an energy-based three-dimensional autopilot. Rashad *et al.*[11] presented a port-Hamiltonian approach for an hexarotor UAV for energy impedance control design. In Souza *et al.*,[12] the passivity-based control of a quadrotor UAV is presented. Meanwhile, In Rashad *etal.*,[13] the port-Hamiltonian modeling of an unmanned aerial vehicle by passivity-based control is shown. Nonlinearity and coupled dynamic systems are important for this research study considering that quadrotor unmanned aerial vehicle posses these nonlinear attributes. Hence, for these reasons, the study by Avazzadeh *et al.*,[14] in which the optimal solution of nonlinear 2D variable order fractional optimal control problem is evinced, is useful for our study.

Other types of unmanned vehicles represented in the port-Hamiltonian formulation are found in studies by Zhou *et al.*,[15] who designed an energy tracking controller for an unmanned surface vessel. In Ma *et al.*,[16] a passivity-based and sliding mode controller for unmanned surface vessels was designed considering uncertainties and disturbances. Lv *et al.*[17] presents an adaptive neural network combined with a port-controlled Hamiltonian framework for unmanned surface vessels subject to input saturation and uncertainties. Meanwhile, in the study by Jin *et al.*,[18] the port-Hamiltonian formulation was implemented for $H - \infty$ controller design of an unmanned underwater vehicle. In the work by Wang *et al.*,[19] the port-Hamiltonian formulation was implemented for unmanned surface vessels by a Fourier-based formation control. In Lv *et al.*,[20] the port-Hamiltonian formulation was implemented for unmanned surface vessels with cooperative formation control.

Neural control has been fundamental for the trajectory tracking control of UAV and other types of robotics mechanisms. So, for this reason, it is worth mentioning the following studies to clarify this issue. For example, in the study by Feng *et al.*,[21] the finite fixed time synchronization of complex variable neural networks was considered. In the work by Jayanthi and Santhakumari,[22] a passivity analysis of complex variable neural networks was evinced. Moreover, in Liu *et al.*[23] a nonpenalty neuro dynamic model for complex variable neural network optimization was presented. In light of the importance of neural network stability for controller design, the study by Sriraman *et al.*[24] was considered.

Other kinds of neural network controllers are presented studies such as Chen *et al.*[25] in which a fuzzy-sliding mode controller UAVs werepresented based on radial basis neural networks. Additionally, Xiong *et al.*[26] envinced a neuro-adaptive sliding mode controller for a tilt quadrotor unmanned aerial vehicle. In the study by Li *et al.*[27] a recurrent neural network with a super-twisting terminal sliding mode controller for UAVs are shown. Chai *et al.*[28] presented an adaptive compensation of a double pendulum aerial transportation system. In the study by Mahmood *et al.*[29] a neural adaptive sliding mode controller for camera positioning of a unmanned aerial vehicle was presented.

Other references for the neural network control of UAV are found in other studies such as Li *et al.*[30] in which a neural network observer was implemented for the fault-tolerant control of an UAV. In the study by Wu *et al.*[31] a neural network and particle swarm optimization technique was implemented for the control for the unmanned aerial vehicle boat landing. In Peng *et al.*[32], the spiking neural control for 12 rotor unmanned aerial vehicle was evinced. Zhang *et al.*[33] presented an adaptive observer based neural control of the swarm of UAV. Additionally, in Bekhiti *et al.*[34] a fixed-wing UAV was controlled with sensor fault recoveries.

The Dirac structures were implemented in this research study due to the structure preservation characteristics of this kind of operator in dynamic systems established in the port-Hamiltonian formulation. Hence, we included studies such as van der Schaft *et al.*[35] in which differential operators and Dirac structures are presented. Meanwhile, Ye *et al.*,[36] presented a generalized

soliton Dirac structure. Furthermore, Yoshimura *et al.*[37] presented the Dirac structures in non-equilibrium thermodynamics. In the work by Kumar *et al.*,[43] the Dirac structures were implemented for linear dynamic systems on Sobolev spaces. In the study by Gay-Balmaz *et al.*,[39] the Dirac structures for interconnected discrete-time systems were evinced.

Moreover, Tortorella *et al.*,[40] reported the deformation of the $L-\infty$ Dirac–Jacobi structure. Seslija *et al.*[41] presented the reduction of Dirac–Stokes operators for port-Hamiltonian systems. Lamoline *et al.*[?] showed the Dirac structures of infinite dimensional stochastic port-Hamiltonian systems.

This paper presents the results of a complex variable neural network (CVNN) controller designed for quadrotor UAVs within a port-Hamiltonian framework. One of the main contributions of this research study is the application of non-holonomic constraints exclusively in the attitude loop, ensuring that the orientation of the unmanned aerial vehicle remains within an appropriate and allowable range. The main motivation of this study is that the position and attitude dynamics of a quadrotor UAV can be decoupled through the use of a Dirac structure. Notably, this approach has not been implemented in previous research. Due to the derivation of the position and attitude dynamics in the form of port-Hamiltonian systems, the non-holonomic constraints make it difficult to obtain a feasible port-Hamiltonian formulation, in specific, for the attitude loop. Hence, the Dirac structure in the attitude loop facilitates the establishment of both loops dynamics in the port-Hamiltonian formulation. The proposed control architecture decouples the attitude and position loops. Both controllers are developed using Lyapunov functionals—the position loop CVNN controller through appropriate Lyapunov selection, and the attitude loop CVNN controller through Lyapunov implementation to derive non-holonomic and input torques. As it is verified, apart from obtaining the port-Hamiltonian dynamics of the attitude and position loops, the main contribution of the proposed control strategy is that the complex variable neural networks provide the framework in which the dynamics in this formulation is obtained by ensuring an appropriate weights of these controllers. This means that the dynamics of the quadrotor UAV is used to derive the CVNN behaviour to reduce the position and attitude errors to zero. It is important to mention that the non-holonomic torque must be kept at its lowest value to prevent constraint violations. This research presents a comprehensive theoretical analysis and experimental validation, followed by a discussion and conclusion.

The novelty of this research study resides in which the non-holonomic constraints of the quadrotor unmanned aerial vehicle are considered, in specific, in the attitude loop. Most studies in the literature overlook these aspects, as they assume a position trajectory without fully accounting for the attitude constraints necessary to define the permissible attitude regions and determine the corresponding rotation angles of the quadrotor UAV.

The non-holonomic constraints considered in this study are incorporated into the attitude controller design to define feasible turning regions for the quadrotor UAV in real-time. This approach enables more realistic control, allowing the implementation of the control strategy for real-time missions regardless of the assigned tasks.

The sections of this paper are summarized as follows. In Section 2, the mathematical background for this research study is presented; in Section 3 the port-Hamiltonian representations of the attitude and position loops are presented. Then, in Section 4, the proposed control approach is established. Meanwhile, in Section 5, two numerical experiments are presented; and finally in Section 6 and Section 7, the respective discussions and conclusions of this research work are evinced.

2. Mathematical background

In this section, the mathematical background of this research study is presented. Specifically, we focus on the definitions of Dirac structures that are essential for the port-Hamiltonian modeling of both attitude and position dynamics of the quadrotor unmanned aerial vehicle.

2.1. Dirac structures

Consider the following bilinear Dirac structure [?,35,37,42,43]

$$\left\langle \begin{pmatrix} f_1 \\ e_1 \end{pmatrix}, \begin{pmatrix} f_2 \\ e_2 \end{pmatrix} \right\rangle = \langle f_1, f_2 \rangle_{\mathcal{F}} + \langle e_1, e_2 \rangle_{\mathcal{E}} \quad (1)$$

in which $(f_1, e_1), (f_2, e_2) \in \mathcal{B}$ for $\mathcal{B} = \mathcal{F} \times \mathcal{E}$, where which $\mathcal{F}$ is the flow space and $\mathcal{E}$ is the effort space.[?,42] Then, any Dirac structure can be established in kernel form[42]:

$$\mathcal{D} = \{(f, e) \in \mathcal{F} \times \mathcal{F}^* : Ff + Ee = 0\} \quad (2)$$

In which the following conditions are met[35,37,42,43]:

i $EF^* + FE^* = 0$
ii $rank[F + E] = dim[\mathcal{F}]$

for linear maps $F : \mathcal{F} \to \mathcal{V}$ and $E : \mathcal{F}^* \to \mathcal{V}$.[42] Meanwhile, every Dirac structure can be established in image representation as shown in Equation 3[42]:

$$\mathcal{D} = \{(f, e) \in \mathcal{F} \times \mathcal{F}^* : f = E^*\lambda, e = F^*\lambda, \lambda \in \mathcal{V} \tag{3}$$

The power variables for each Dirac structure are given[42]:

$$P = \langle f^* | f \rangle \tag{4}$$

in which $(f, f^*) \in \mathcal{F} \times \mathcal{F}^*$.[42]

The Dirac structure is a compact and suitable operator to obtain the port-Hamiltonian formulation of the attitude and position dynamics. Considering that the attitude dynamics is nonlinear and coupled, due to its complexity, the Dirac structure becomes in a compact form which ease the dynamic model derivation, not only in the attitude loop, but also in the position loop.

2.2. Euler angles' matrices and coordinate transformation

The Euler angles matrices, along with coordinate transformation, are shown in this subsection. Consider the following transformation[44]:

$$R_0 = SR_B \tag{5}$$

in which the Euler angles are given by:

$$R_B = \begin{pmatrix} C_\Psi C_\Theta & S_\Theta S_\Phi C_\Psi - S_\Psi C_\Phi & C_\Phi C_\Psi S_\Theta + S_\Phi S_\Psi \\ C_\Theta S_\Psi & S_\Phi S_\Psi S_\Theta + C_\Phi S_\Psi & C_\Phi S_\Psi S_\Theta - S_\Phi C_\Psi \\ -S_\Theta & S_\Phi C_\Theta & C_\Phi C_\Theta \end{pmatrix} \tag{6}$$

where S and C are the sine and cosine functions, and $\gamma = [\Phi, \Theta, \Psi]^T$ are the respective Euler angles. Meanwhile the skew symmetric matrix S is given by Equation 7[44]:

$$S = \begin{pmatrix} 0 & \Omega_r & \Omega_q \\ -\Omega_r & 0 & \Omega_p \\ -\Omega_q & -\Omega_p & 0 \end{pmatrix} \tag{7}$$

where $\Omega = [\Omega_p, \Omega_q, \Omega_r]^T$ represents the angular velocities around the x, y, and z axes. The relation between γ and Ω is given by Equation 8[44]:

$$\dot{\gamma} = \begin{pmatrix} 1 & \tan(\Theta)\sin\Phi & \tan\Theta\cos(\Phi) \\ 0 & \cos(\Phi) & -\sin(\Phi) \\ 0 & \sec\Theta\sin\Phi & \sec\Theta\cos\Phi \end{pmatrix} \Omega \tag{8}$$

Now, to find the input torques of the propellers T_i for $i = 1, 2, 3, 4$, the following transformation is necessary:

$$\begin{bmatrix} R_B & R_B & R_B & R_B \end{bmatrix}^{-1} f_x = V \tag{9}$$

in which $V = [V_1, V_2, V_3, V_4]^T$ for $V_1 = [0, 0, T_1]^T$, $V_2 = [0, 0, T_2]^T$, $V_3 = [0, 0, T_3]^T$, and $V_4 = [0, 0, T_4]^T$. Equation 8 is used to transform the attitude orientation of the quadrotor UAVs to the Euler angles.

3. Port-Hamiltonian representation of the quadrotor unmanned aerial vehicles

As explained in the previous section, the position and attitude dynamics of the quadrotor unmanned aerial vehicle are decoupled and represented in the port-Hamiltonian formulation by Dirac structures. First, a flow vector and an effort vector are developed to implement the Dirac structure to establish the position and attitude dynamics in the port-Hamiltonian formulation. It is important to consider that the non-holonomic constraints in the attitude loop are taken into consideration. This means that constraints are applied only to the rotation angles of the unmanned aerial vehicle when tracking a desired position. To represent the unmanned aerial vehicle attitude dynamics in the port-Hamiltonian formulation, consider the following port-Hamiltonian formulation[45]:

$$\begin{aligned} \dot{q}_a &= \nabla_{p_a} H(q_a, p_a) \\ \dot{p}_a &= -\nabla_{q_a} H(q_a, p_a) + A(q_a)\lambda + B(q_a)u_a \\ y_a &= B(q_a)^T \nabla_{p_a} H(q_a, p_a) \\ 0 &= A(q_a)^T \nabla_{p_a} H(q_a, p_a) \end{aligned} \tag{10}$$

where ∇_{q_a} is the partial gradient with respect to q_a, ∇_{p_a} is the partial gradient with respect to p_a, $q_a \in \mathbb{R}^3$ is the orientation vector, $p_a \in \mathbb{R}^3$ is the momentum vector, $H(q_a, p_a) : \mathbb{R}^3 \to \mathbb{R}$ is the Hamiltonian for the attitude loop, $A(q_a)\lambda$ is the constrained torque, $B(q_a)u_a$ is the input torque,[45] and $y_a \in \mathbb{R}^3$ is the system output. The Dirac structure used in this paper is considered as:

$$\langle f | e \rangle + \langle f_a | e_a \rangle + \langle f_c | e_c \rangle = 0 \tag{11}$$

where $f = -\dot{x}(t)$ and $e = \frac{\partial H(x)}{\partial x}$, $f_a = -\dot{x_a}(t)$, $e_a = u_a$, $f_c = -\dot{x_c}(t)$, $e_c = \lambda$. The vector $x(t) = [q_a(t), p_a(t)]^T$ is the state vector. It is worthy to mention that $\dot{x}_a$ is the velocity generated by the controller input, $\dot{x}_c$ is the velocity obtained by the constraint torque, $e_a = u_a$ is the torque generated

by the controller input, and $e_c = \lambda$ is the torque generated by the constraints.

Equation 11 is converted to the following result, considering the kernel property of the Dirac structure:

$$-F\dot{x}(t) + E\frac{\partial H}{\partial x} + F_a f_a + E_a e_a + F_c f_c + E_c e_c = 0 \quad (12)$$

Hence, by making $F = I_n$, $E = J$, $F_c = F_a = 0_n$, $E_a = B(q_a)$, and $E_c = A(q_a)$; the previous equation becomes:

$$\begin{aligned} \dot{x}(t) &= J\frac{\partial H(q_a(t), p_a(t))}{\partial x(t)} + G(q_a(t))u_a(t) \\ &+ A(q_a(t))\lambda(t) \end{aligned} \quad (13)$$

which is the same port-Hamiltonian formulation as evinced in Equation 10.

Meanwhile, the position loop in the port-Hamiltonian formulation is given by:

$$\begin{aligned} \dot{q}_x &= \nabla_{p_x} H(q_x, p_x) \\ \dot{p}_x &= -\nabla_{q_x} H(q_x, p_x) + B(q_x)u_x \\ y_x &= B(q_x)^T \nabla_{p_x} H(q_x, p_x) \end{aligned} \quad (14)$$

Similar to the attitude loop, Equation 14 can be represented by Dirac structures as follows:

$$\langle f|e\rangle + \langle f_x|e_x\rangle = 0 \quad (15)$$

Obtaining the following by the kernel property gives:

$$-F\dot{x}(t) + E\frac{\partial H}{\partial x} + F_x f_x + E_x e_x = 0 \quad (16)$$

where $F : \mathbb{R}^{6\times 6} \to \mathbb{R}^6$ is the flow matrix and $E : \mathbb{R}^{6\times 6} \to \mathbb{R}^6$ is the effort matrix. The vector $x(t) = [q_x(t), p_x(t)]^T$ is the state vector, making $F = I_n$, $E = J$, $F_x = 0_n$, and $E_x = B(q_x)$ in which $n = 6$; the previous equation becomes:

$$\dot{x}(t) = J\frac{\partial H(q_x(t), p_x(t))}{\partial x(t)} + G(q_x(t))u_x(t) \quad (17)$$

In this way, we have demonstrated how both the attitude and position dynamics are synthesized through the implementation of Dirac structures, providing a unified and elegant mathematical framework.

3.1. Port-Hamiltonian representation of the quadrotor's position loop

For the position loop dynamics, we followed a similar approach to the previous demonstration, implementing the Dirac structure to obtain the port-Hamiltonian formulation. Consider the following unmanned aerial vehicle position vector $q_x = [x, y, z]^T$ along with the momentum vector in the x,y, and z axes $p_p = [p_x, p_y, p_z]^T$. Additionally, consider the following mass matrix:

$$M = \begin{bmatrix} m & 0 & 0 \\ 0 & m & 0 \\ 0 & 0 & m \end{bmatrix} \quad (18)$$

in which m is the mass of the quadrotor. Now, consider the following Hamiltonian for the position loop [44]:

$$H_x = \frac{1}{2}p_p^T M^{-1} p_p + Mg\epsilon_3 q_x \quad (19)$$

where, the kinetic energy is given by $K = \frac{1}{2}p_p^T M^{-1} p_p$ and the potential energy is given by $P = Mg\epsilon_3 q_x$ in which g is the gravity constant, $\epsilon_3 = [0, 0, 1]^T$. Then, consider the following partial derivatives of the Hamiltonian H_x:

$$\begin{aligned} \frac{\partial H_x}{\partial q_x} &= Mg\epsilon_3 \\ \frac{\partial H_x}{\partial p_p} &= M^{-1}p_p = M^{-1}(M\dot{q}_x) = \dot{q}_x \end{aligned} \quad (20)$$

So, according to Equation 14, the port-Hamiltonian formulation for the position loop is given as:

$$\begin{bmatrix} \dot{q}_x \\ \dot{p}_p \end{bmatrix} = \begin{bmatrix} 0_3 & I_3 \\ -I_3 & 0 \end{bmatrix} \begin{bmatrix} Mg\epsilon_3 \\ \dot{q}_x \end{bmatrix} + Bu_x \quad (21)$$

where $u_x = [0, 0, 0, u_1, u_2, u_3]^T$ is the system input. Meanwhile, B is an identity matrix of the appropriate dimension.

3.2. Port-Hamiltonian representation of the quadrotor's attitude loop

For the attitude dynamics loop, we implemented a similar procedure to obtain the port-Hamiltonian formulation. Consider the following Hamiltonian with the kinetic and potential energy[44]:

$$H_a = \frac{1}{2}p_a^T J_B^{-1} p_a + \int_{q_a} \dot{q}_a \times J_B \dot{q}_a dq_a \quad (22)$$

The integral term which appears in Equation 22 represents the potential energy of the quadrotor unmanned aerial vehicle, this means, that this integral represents the accumulated potential energy related to the respective torque. Considering the following variables $q_a = [a_1, a_2, a_3]^T$ in which a_1, a_2, and a_3 are the rotation angles of the unmanned aerial vehicle in the x, y, and z axes. Meanwhile, $p_a = [p_{ax}, p_{ay}, p_{az}]^T$ is the angular momentum vector. Then, the inertia matrix is given by:

$$J_B = \begin{bmatrix} I_{xx} & 0 & 0 \\ 0 & I_{yy} & 0 \\ 0 & 0 & I_{zz} \end{bmatrix} \quad (23)$$

where I_{xx}, I_{yy}, and I_{zz} are the inertia in the x, y, and z axes, respectively. Now, consider the following partial derivatives of the attitude Hamiltonian:

$$\begin{aligned} \frac{\partial H_a}{\partial q_a} &= \dot{q}_a \times J_B \dot{q}_a \\ \frac{\partial H_a}{\partial p_a} &= J_B^{-1} p_a = J_B^{-1}(J_B \dot{q}_a) = \dot{q}_a \end{aligned} \quad (24)$$

So, according to Equation 10, the attitude dynamics in the port-Hamiltonian formulation are given by:

$$\begin{aligned} \begin{bmatrix} \dot{q}_a \\ \dot{p}_a \end{bmatrix} &= \begin{bmatrix} 0_3 & I_3 \\ -I_3 & 0 \end{bmatrix} \begin{bmatrix} \dot{q}_a \times J_B \dot{q}_a \\ \dot{q}_a \end{bmatrix} \\ &+ \begin{bmatrix} 0 \\ A(q_a)\lambda \end{bmatrix} + B_a u_a \end{aligned} \quad (25)$$

where $u_a = [0, 0, 0, u_{ax}, u_{ay}, u_{az}]^T$ is the input torque vector, and B_a is an identity matrix of appropriate dimensions. The constraints matrix elements are obtained by Cholesky factorization as follows:

$$\begin{aligned} A^T(q_a)\frac{\partial H_a}{\partial p_a} &= 0 \\ A^T(q_a)\dot{q}_a &= 0 \\ R(q_a)(R^T(q_a)\dot{q}_a) &= 0 \end{aligned} \quad (26)$$

in which the Cholesky factorization is given by $A(q_a) = R(q_a)R^T(q_a)$; hence, $R^T(q_a)$ is found by implementing a solver. The main reason that the Cholesky factorization was implemented, is to facilitate the calculation of the non-holonomic constraints. Due to these constraints, the unmanned aerial vehicle quadrotor dynamics consider non-allowed positions of the UAV itself. Hence, to be non-holonomic constraints, the elements of the matrix $A^T(q_a)$ are found numerically when the non-holonomic conditions are met.

To clarify how the non-holonomic constraints are found by the Cholesky factorization of $A^T(q_a)$, consider it in Equation 26, where the computation effort is reduced if only $R(q_a) = 0$ or the product of $R^T(q_a)\dot{q}_a = 0$. In summary, the Cholesky factorization was implemented mostly to reduce the computation effort in a real-time hardware implementation of the quadrotor UAV's dynamic system.

4. Complex variable neural network controller for the quadrotor unmanned aerial vehicle

In this section, the complex variable neural networks controllers are obtained. It is important to remark that by decoupling the position and attitude loops makes it easy to design the two complex variable neural network controllers for the unmanned aerial vehicle. As explained in the previous section, the establishment of the separated position and attitude loops provides an easiest way to design the separated controllers to guarantee a precise trajectory tracking control. Firstly, the controller in the position loop is obtained and then this loop generates the trajectories for the attitude loop by a transformation, as seen in Figure 1.

The complex variable neural network component is given as Equation 27 [46]:

$$\dot{x}_{ci}(t) = -dx_{ci}(t) + f(x_{ci}) + c\sum_{j=1}^{n} a_{ij}\Gamma x_{cj} + u_{nni} \quad (27)$$

where $\Gamma = diag\{h_1, ..., h_n\} \in \mathbb{C}^{n\times n}$, $d = diag\{h_1, ..., h_n\} \in \mathbb{C}^{n\times n}$, $c \in$ is the coupling strength, and $A = \{a_{ij}\}_{N\times N}$ is the weight matrix with $a_{ij} \in \mathbb{C}$.[46] The complex variable neural network structure given in Equation 27 was implemented in the attitude and position loop controllers, see (Figure 1), as explained later in this section.

The following property is important to clarify the bounds of the nonlinear complex variable neural network terms.

Property 1. *Consider the following nonlinear term of the complex variable neural network $f(x_{ci}) \in \mathbb{C}^n$. This term posses the following upper bound property:*

$$\|f(x_{ci})\| \leq \alpha \quad (28)$$

where $\alpha \in \mathbb{R}^+$ is a positive constant.

With this property, the attitude and position loops controllers are designed effectively considering the bounded characteristics of the neural network nonlinear term $f(x_{ci})$.

4.1. Complex variable neural network controller design of the position loop

For the position trajectory control tracking, consider the following error variables:

$$\begin{aligned} e_{iq} &= q_{xdi} - q_{xi} \\ e_{ip} &= p_{xdi} - p_{xi} \end{aligned} \quad (29)$$

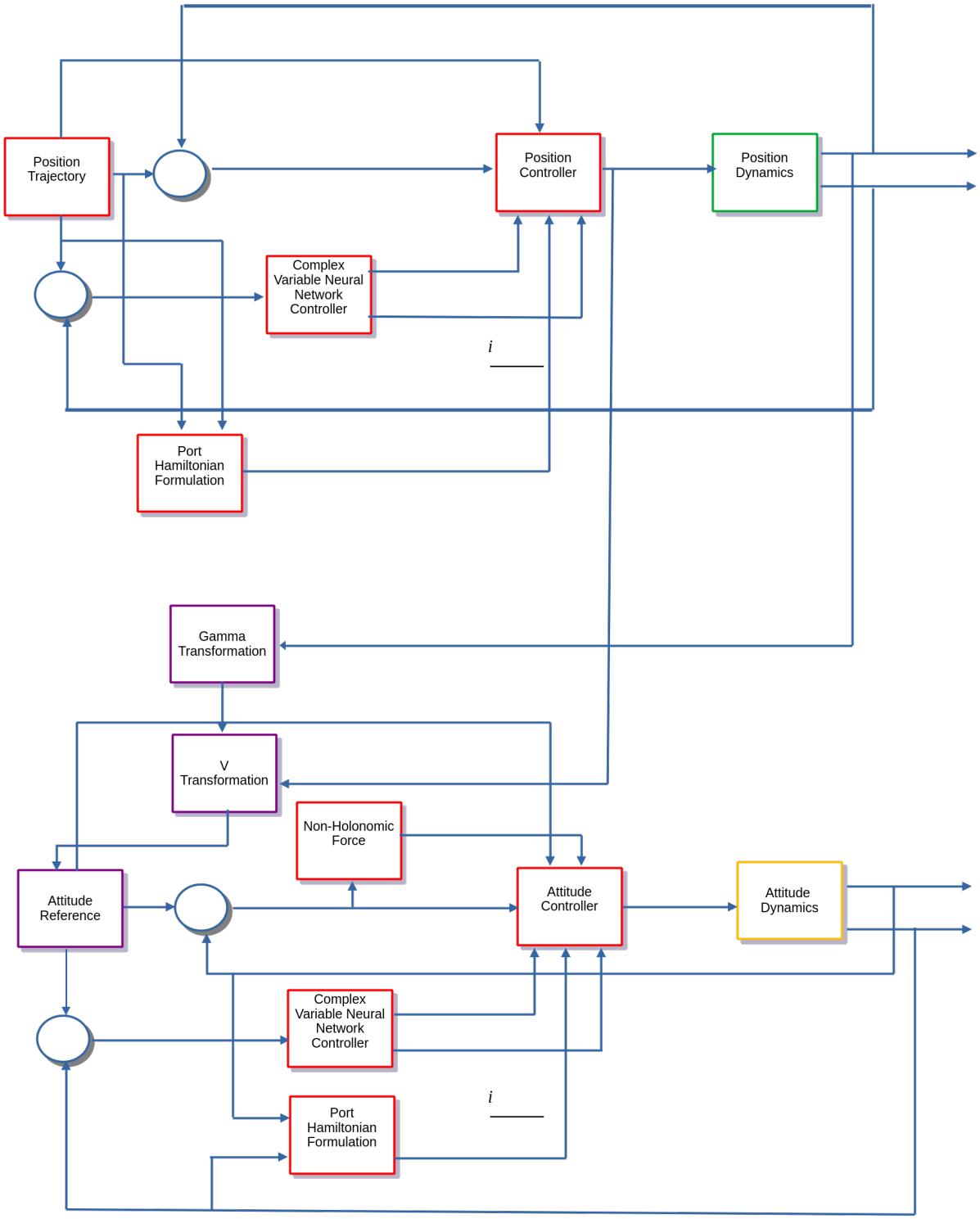

Figure 1. Block diagram of the proposed control strategy

in which q_{xdi}, and p_{xdi} are the desired position and momentum in the x, y and z frames respectively for $i = 1, 2, 3$. The following theorem presents the derivation of the position loop complex variable neural network controller:

Theorem 1. *Consider the controlled port-Hamiltonian formulation of the position loop given in Equation 21. The trajectory tracking of the position to drive the error variables in Equation 29 to the origin in finite time, if and only if, the following control law is implemented:*

$$\begin{aligned} u_i &= \dot{p}_{dxi} + \frac{\partial H_{xi}}{\partial q_{xi}} + \dot{e}_{iq} + x_{c\mathbb{R}i}\dot{x}_{c\mathbb{R}i} \\ &+ x_{c\mathbb{I}i}\dot{x}_{c\mathbb{I}i} + K_{1xi}e_{iq}^2 + K_{2xi}e_{ip}^2 \end{aligned} \quad (30)$$

where $x_{c\mathbb{R}i} \in \mathbb{R}$ and $x_{c\mathbb{I}i} \in \mathbb{R}$ are the real and complex components of the complex variable neural network controller in Equation 27. Meanwhile, $K_{1xi} \in \mathbb{R}^+$ and $K_{2xi} \in \mathbb{R}^+$ are the respective gain matrices.

Proof. Consider the following Lyapunov function:

$$W = \sum_{i=1}^{3} |e_{iq}| + \sum_{i=1}^{3} |e_{ip}| + \frac{1}{2} x_{c\mathbb{R}}^T x_{c\mathbb{R}} + \frac{1}{2} x_{c\mathbb{I}}^T x_{c\mathbb{I}} \tag{31}$$

Now, by taking the first time derivative of Equation 31, the following result is obtained:

$$\begin{aligned} \dot{W} &= \sum_{i=1}^{3} \dot{e}_{iq} + \sum_{i=1}^{3} \dot{e}_{ip} + \sum_{i=1}^{3} x_{c\mathbb{R}i} \dot{x}_{c\mathbb{R}i} \\ &+ \sum_{i=1}^{3} x_{c\mathbb{I}i} \dot{x}_{c\mathbb{I}i} \end{aligned} \tag{32}$$

Now, by substituting the elements of Equation 21 into Equation 32 the following result is obtained:

$$\begin{aligned} \dot{W} &= \sum_{i=1}^{3} \dot{e}_{iq} + \sum_{i=1}^{3} \left(\dot{p}_{dxi} + \frac{\partial H_{xi}}{\partial q_{xi}} - u_i \right) \\ &+ \sum_{i=1}^{3} x_{c\mathbb{R}i} \dot{x}_{c\mathbb{R}i} + \sum_{i=1}^{3} x_{c\mathbb{I}i} \dot{x}_{c\mathbb{I}i} \end{aligned} \tag{33}$$

Now, by substituting the control law in Equation 30 into Equation 33 the following result is obtained:

$$\dot{W} = -\sum_{i=1}^{3} (K_{1xi} e_{iq}^2 + K_{2xi} e_{ip}^2) < 0 \tag{34}$$

Hence, the position loop is closed-loop stable, and the proof of the theorem is complete.

4.2. Complex variable neural network controller design of the attitude loop

For the design of the complex variable neural controller for the attitude loop, a similar procedure was followed. Consider the following error variables:

$$\begin{aligned} e_{iq} &= q_{di} - q_{ai} \\ e_{ip} &= p_{di} - p_{ai} \end{aligned} \tag{35}$$

in which e_{iq} and e_{ip} are the angular orientation and angular momentum error variables for $i = 1, 2, 3$. The following theorem demonstrates how the control input variable was synthesized.

Theorem 2. *Consider the error variables described in Equation 35 and the controlled port-Hamiltonian formulation of the attitude position in Equation 25, this nonlinear dynamic system is stabilized, if and only if, the following control and constraint inputs are implemented in Equation 25:*

$$\begin{aligned} u_{ai} &= \dot{p}_{di} + \frac{\partial H_{ai}}{\partial q_{ai}} + K_{1a} e_{iq}^2 \\ &+ K_{2a} e_{ip}^2 + x_{c\mathbb{R}i} \dot{x}_{c\mathbb{I}i} + x_{c\mathbb{I}i} \\ \lambda_i &= \frac{1}{\|a_i\|} (a_i)^T \dot{e}_{iq} \end{aligned} \tag{36}$$

where $K_{1a} \in \mathbb{R}^+$, $K_{2a} \in \mathbb{R}^+$ are positive constant gains, and $x_{c\mathbb{R}i} \in \mathbb{R}$ and $x_{c\mathbb{I}i} \in \mathbb{R}$ are the real and imaginary components of the complex variable neural network controller. Meanwhile, a_i is the row vector of the matrix $A(q_a)$ related to the non-holonomic constraints of the system.

Proof. Consider the following Lyapunov function:

$$\begin{aligned} W &= \sum_{i=1}^{3} |e_{iq}| + \sum_{i=1}^{3} |e_{ip}| \\ &+ \frac{1}{2} \sum_{i=1}^{3} x_{c\mathbb{R}i}^2 + \frac{1}{2} \sum_{i=1}^{3} x_{c\mathbb{I}i}^2 \end{aligned} \tag{37}$$

By obtaining the first time derivative of the Lyapunov functional Equation (37), the following result is obtained:

$$\begin{aligned} \dot{W} &= \sum_{i=1}^{3} (\dot{q}_{di} - \dot{q}_{ai}) + \sum_{i=1}^{3} (\dot{p}_{di} - \dot{p}_{ai}) \\ &+ \sum_{i=1}^{3} x_{c\mathbb{R}i} \dot{x}_{c\mathbb{R}i} + \sum_{i=1}^{3} x_{c\mathbb{I}i} \dot{x}_{c\mathbb{I}i} \end{aligned} \tag{38}$$

Now implementing the required substitutions in Equation (38), we obtain:

$$\begin{aligned} \dot{W} &= \sum_{i=1}^{3} (\dot{q}_{di} - \dot{q}_{ai}) \\ &+ \sum_{i=1}^{3} \left(\dot{p}_{di} + \frac{\partial H_{ai}}{\partial q_{ai}} - a_i \lambda_i - u_{ai} \right) \\ &+ \sum_{i=1}^{3} x_{c\mathbb{R}i} \dot{x}_{c\mathbb{R}i} + \sum_{i=1}^{3} x_{c\mathbb{I}i} \dot{x}_{c\mathbb{I}i} \end{aligned} \tag{39}$$

Now by substituting λ and u_{ai} in Equation (36) the following result is obtained:

$$\dot{W} = -\sum_{i=1}^{3} \left(-K_{1ai} e_{iq}^2 - K_{2ai} e_{ip}^2\right) < 0 \qquad (40)$$

With these results, the proof is completed and the theorem is established.

5. Numerical experiment

In this numerical experiment section, two numerical experiments are shown in which the first one is related to a trajectory path with aggresive maneuvering and a second scenario in which a smooth trajectory is provided to test the efficiency of the proposed control strategy in comparison with the strategy shown in[47] and a proportional derivative (PD) controller. Meanwhile, the parameters of the quadrotor unmanned aerial vehicle are as follows: $m = 1\ kg$, $g = 9.81\ m/s^2$, with the following inertia matrix:

$$J_B = \begin{pmatrix} 1000 & 0 & 0 \\ 0 & 1000 & 0 \\ 0 & 0 & 1000 \end{pmatrix} \qquad (41)$$

where the unit of the inertia matrix J_B is given in $kg.m^2$. The main objective of this research study is to validate the theoretical results obtained in this research study and, at the same time, to demonstrate the effects of non-holonomic constraints in the dynamics and control of the unmanned aerial vehicle. This section is divided into two parts, which are the following:

i Numerical simulation of the position loop.
ii Numerical simulation of the attitude loop.

This organization improves the comprehension of this section to establish comprehensive validation of the theoretical framework developed in this research.

5.1. Experiment 1

This numerical experiment presents the results of path trajectory tracking for the modeled UAV during aggressive maneuvers. A desired position vector is implemented as the desired trajectory of the unmanned aerial vehicle to test and validate the theoretical results obtained in this research study. The simulation parameters are as explained in the beginning of this section. The simulation analysis is divided into the closed-loop numerical simulation of the position loop and the closed-loop numerical simulation of the attitude loop.

5.1.1. Numerical Simulation of the Position Loop

For this numerical simulation, the gain values for the controller of the neural network controller were given by $K_1 = 0.4$ and $K_2 = 1 \times 10^{-4}$ to achieve a precise trajectory tracking by the studied unmanned aerial vehicle. The results of this numerical simulation experiment were compared with the results obtained by Singha et al.[47] and a standard PD controller. A comparative table of the root mean square error (RMSE) of the three control strategies is presented. It is important to clarify that the strategy shown by Singha et al.[47] was adapted to the dynamics in the port-Hamiltonian formulation of the unmanned aerial vehicle developed in this research study.

In Figures 2 and 3 show the respective evolution in time of the position and error variables in this numerical experiment. It can be noticed that the results obtained by the proposed control strategy provided a better trajectory tracking performance in comparison with the results obtained with the adapted control strategy shown in[47] and the standard PD controller. It is also important to clarify that these results were not affected by the constraints established in the unmanned aerial vehicle presented in this research study, something that can be noticed in the analysis shown in the simulation of the attitude loop, as evidenced in this numerical experiment.

Meanwhile, Figure 4 demonstrates the control inputs of the position variables to verify was obtained without saturating the actuators, as corroborated in the numerical simulation of the attitude loop as shown in this numerical simulation section.

5.1.2. Numerical Simulation of the Attitude Loop

For the numerical simulation of the attitude loop system, the gain of the controller was given by $K_1 = 58$; hence, it is verified in this numerical experiment that the control strategy yielded in this research study provides the best results in comparison with the adapted control strategy shown by Singha et al.[47] and a standard PD controller. Later in this section, a table with the resulting RMSEs is presented to verify which of the controller strategies provide the optimal performance.

Figure 5 shows the angular momentums in the x, y, z axes. It is important to consider that these angular momentums were related directly with the angular velocities of the analyzed unmanned aerial vehicle. This fact is verified

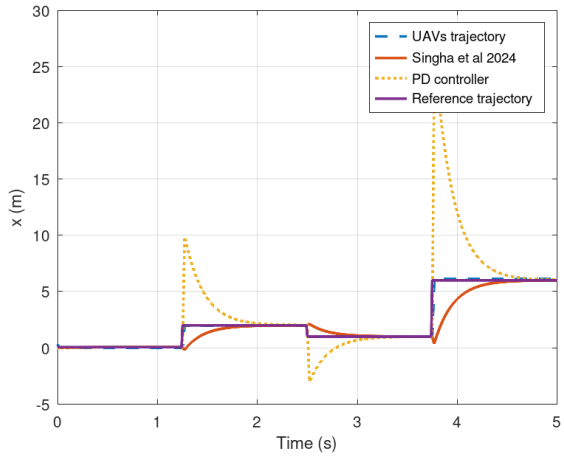

A

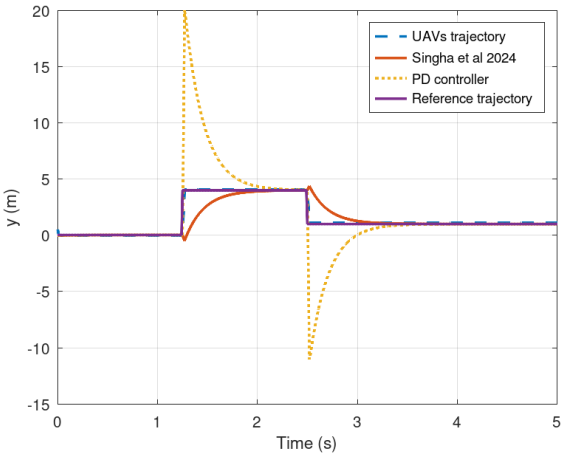

B

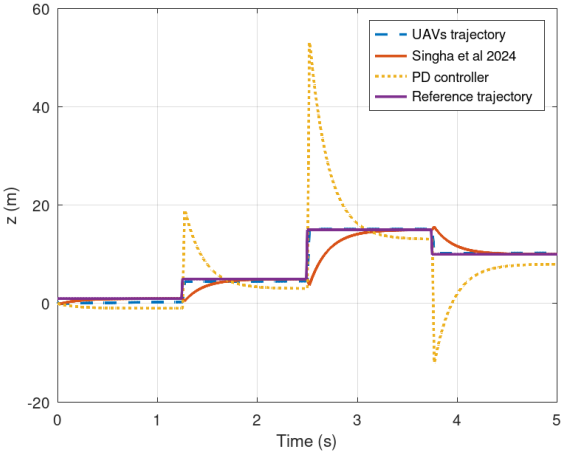

C

Figure 2. Position trajectory in the x, y, and z (A) x, (B) y, and (C) z axes
Abbreviations: PD: Proportional derivative; UAV: Unmanned aerial vehicle.

later the following figure. It is noticeable how the constraints were maintained for these state variables of the unmanned aerial vehicle nonlinear dynamics.

Figure 6 shows the evolution in time of the errors of the angular velocity of the constrained unmanned aerial vehicle studied in this research study. It is corroborated that the optimal results were obtained with the proposed control strategy in comparison with the results of Singha et al.[47] and the PD controller. These results are corroborated later in Table 1.

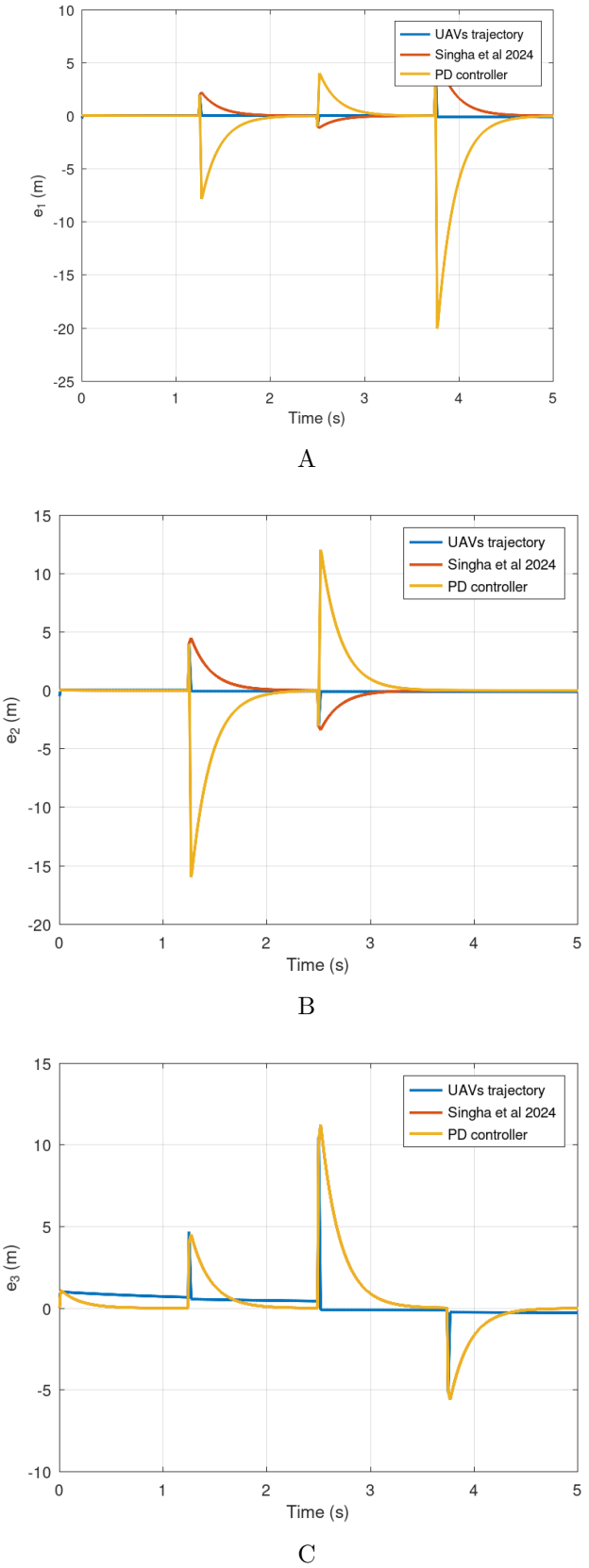

Figure 3. Position error in the (A)x, (B)y, and (C)z axes
Abbreviations: PD: Proportional derivative; UAV: Unmanned aerial vehicle.

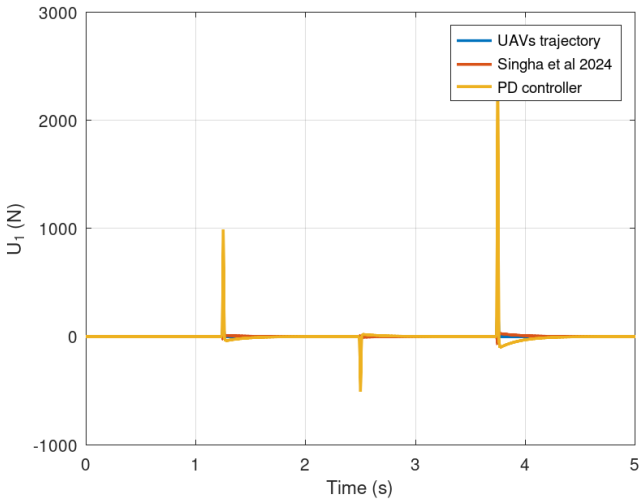

A

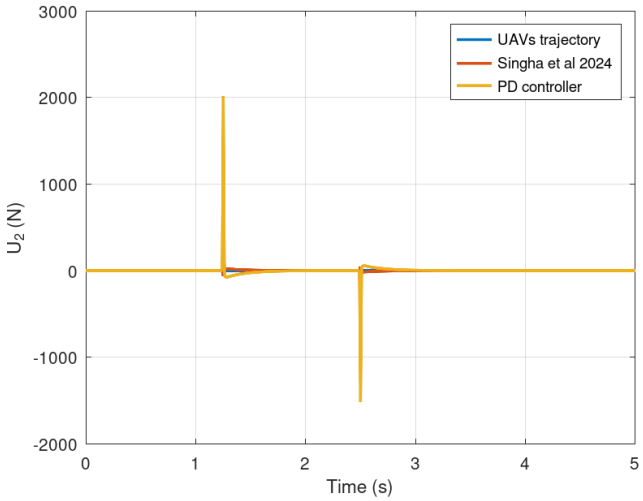

B

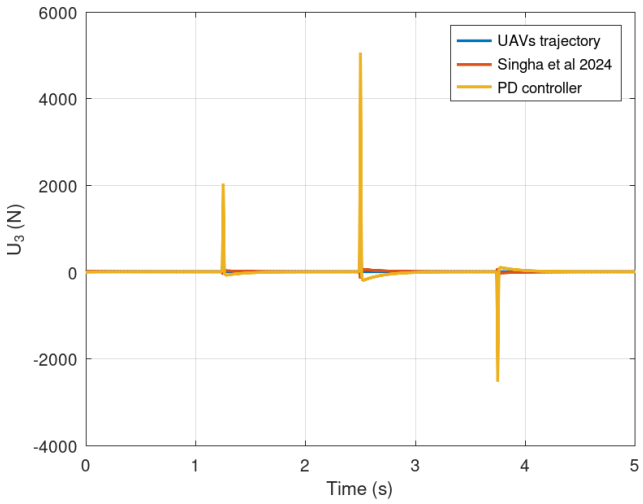

C

Figure 4. Input variables in the(A)x, (B)y, and (C)z axes
Abbreviations: PD: Proportional derivative; UAV: Unmanned aerial vehicle.

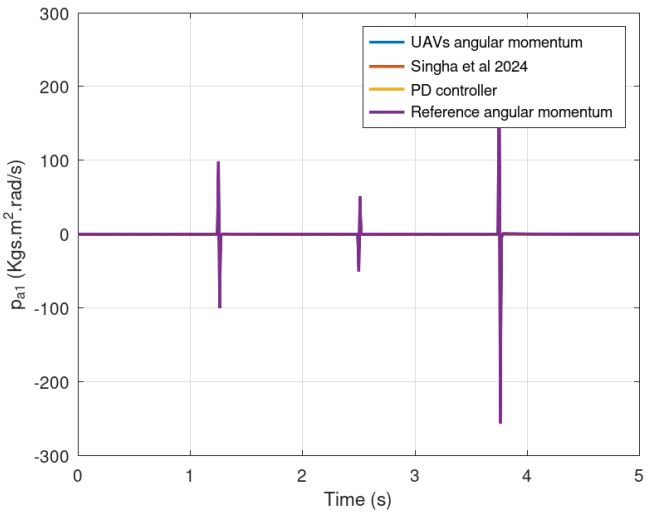

A

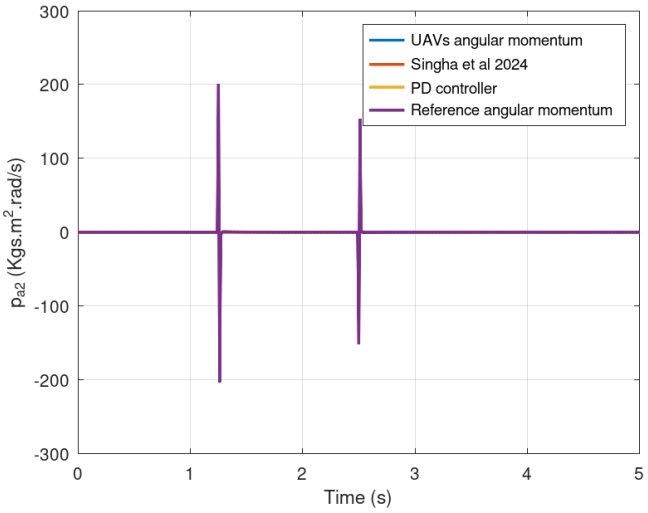

B

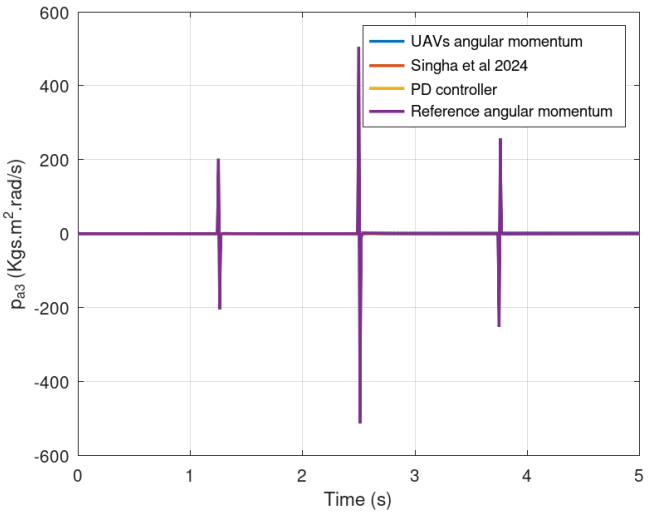

C

Figure 5. Angular momentum trajectory in the (A) x, (B) y, and (C) z axes Abbreviations: PD: Proportional derivative; UAV: Unmanned aerial vehicle.

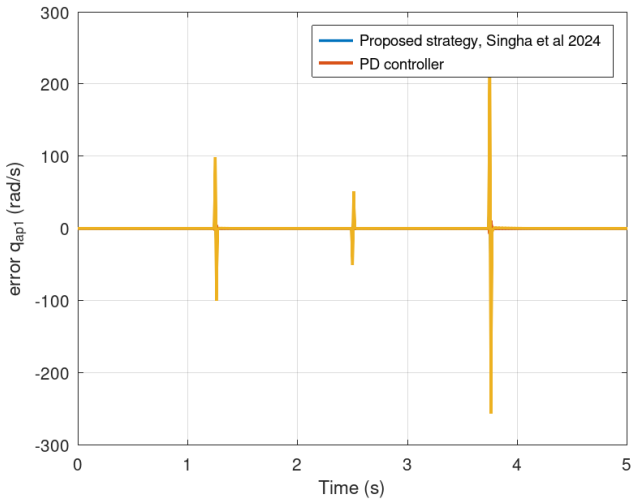

A

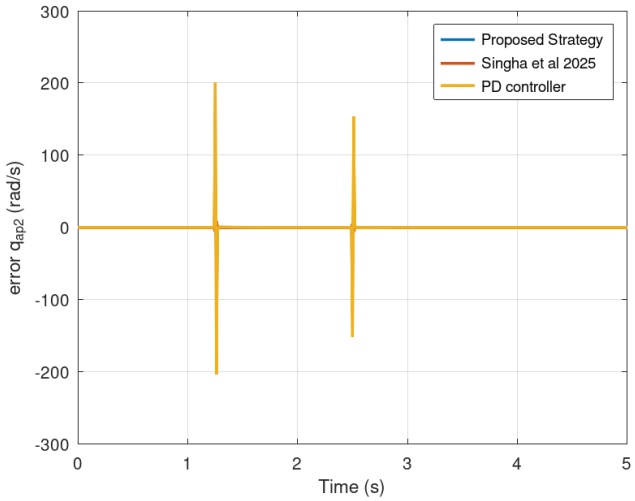

B

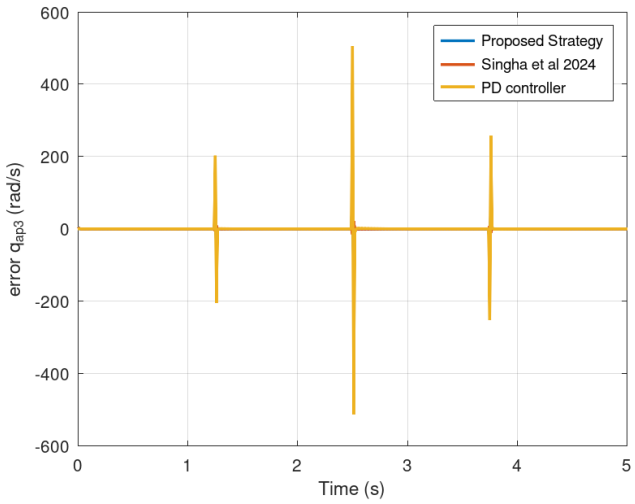

C

Figure 6. Error of the angular velocity in the (A)x, (B)y, and (C)z axes
Abbreviations: PD: Proportional derivative; UAV: Unmanned aerial vehicle.

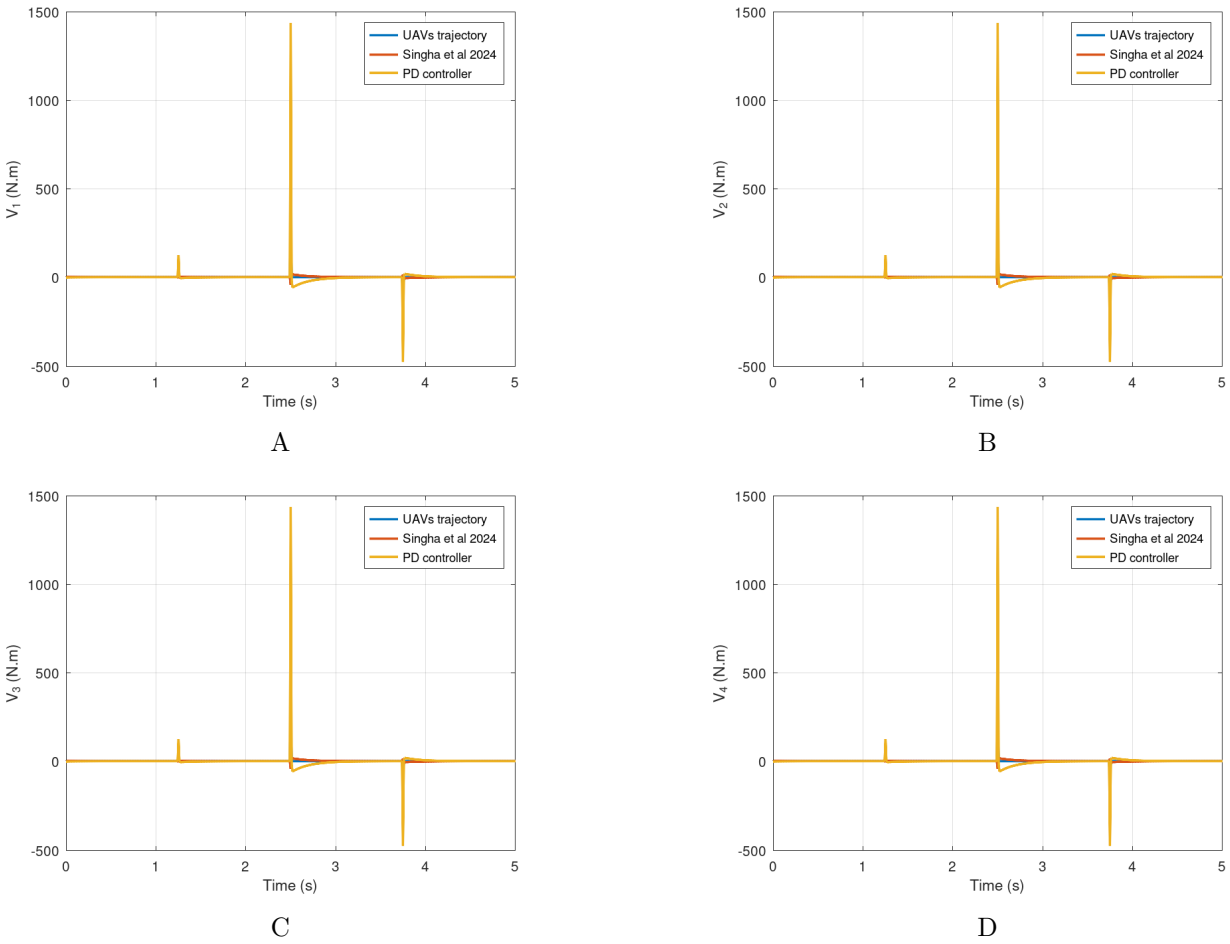

Figure 7. Torque of the four rotors of the quadrotor unmanned aerial Torque of rotor (A) 1, (B) 2, (C) 3, and (D) 4 vehicle
Abbreviations: PD: Proportional derivative; UAV: Unmanned aerial vehicle.

Table 1. Comparison of root mean square errors from different strategies for Experiment 1

Variables	Normalized values of the root mean square error
(Position) Proposed approach	0.8900 m
(Position)(Singha et al., 2024)[47]	2.4105 m
(Position) Proportional derivative controller	8.0149 m
(Attitude) Proposed approach	0.065056 rads
(Attitude) (Singha et al., 2024)[47]	0.018947 rads
(Attitude) Proportional derivative controller	0.3184 rads

Table 2. Mean comparative table for the performance different strategies for Experiment 1

Variables	Proposed approach	(Singha et al., 2024)[47]	Proportional derivative controller
x (m)	0.016470	0.2867	–0.9470
y (m)	–0.066614	0.047745	–0.1557
z (m)	0.2588	0.4753	0.4853
a_1 (rad)	1.1607×10^{-3}	1.1960×10^{-3}	1.2034×10^{-3}
a_2 (rad)	1.2760×10^{-4}	1.9960×10^{-4}	1.9960×10^{-4}
a_3 (rad)	0.011388	0.011808	0.011409

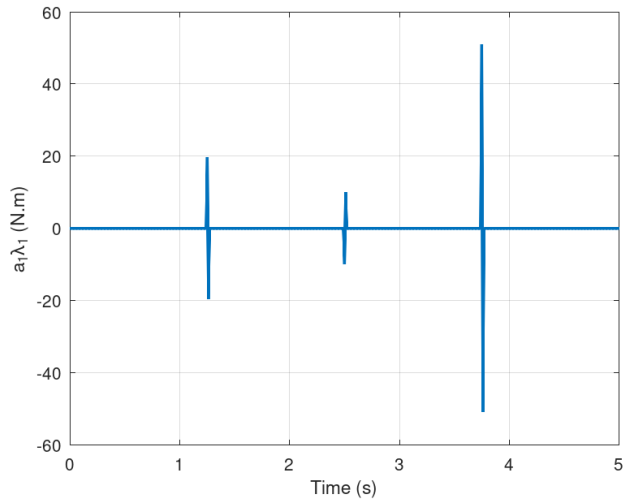

A

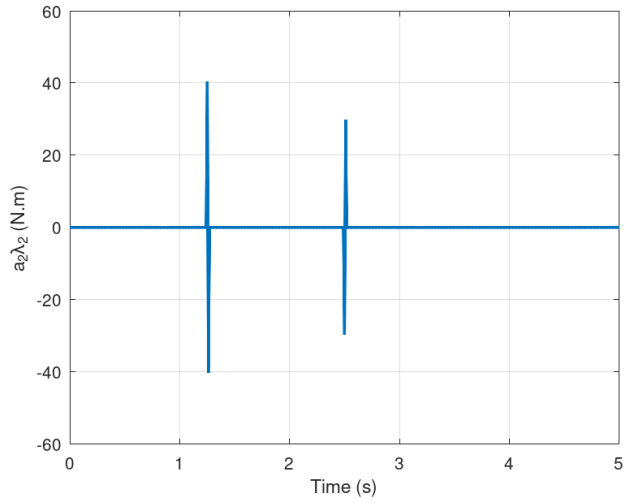

B

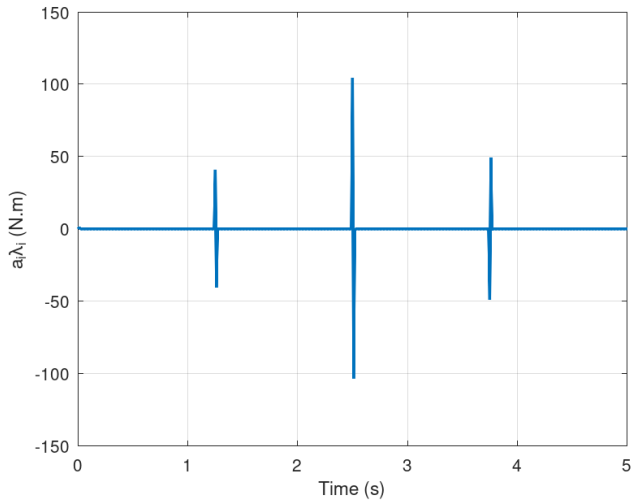

C

Figure 8. Constrained inputs with the calculation of $A(q)\lambda$ (A) x, (B) y, and (C) z axes
Abbreviations: PD: Proportional derivative; UAV: Unmanned aerial vehicle.

Table 3. Variance comparative table for the performance of different strategies for Experiment 1

Variables	Proposed approach	(Singha et al., 2024)[47]	Proportional derivative controller
x (m)	0.078588	0.8005	9.1974
y (m)	0.067362	0.7330	8.3849
z (m)	0.5758	3.9778	45.625
a_1 (rad)	6.1616×10^{-4}	3.2564×10^{-5}	0.015451
a_2 (rad)	5.0271×10^{-4}	2.8287×10^{-5}	0.012880
a_3 (rad)	2.9906×10^{-4}	1.5770×10^{-4}	0.073103

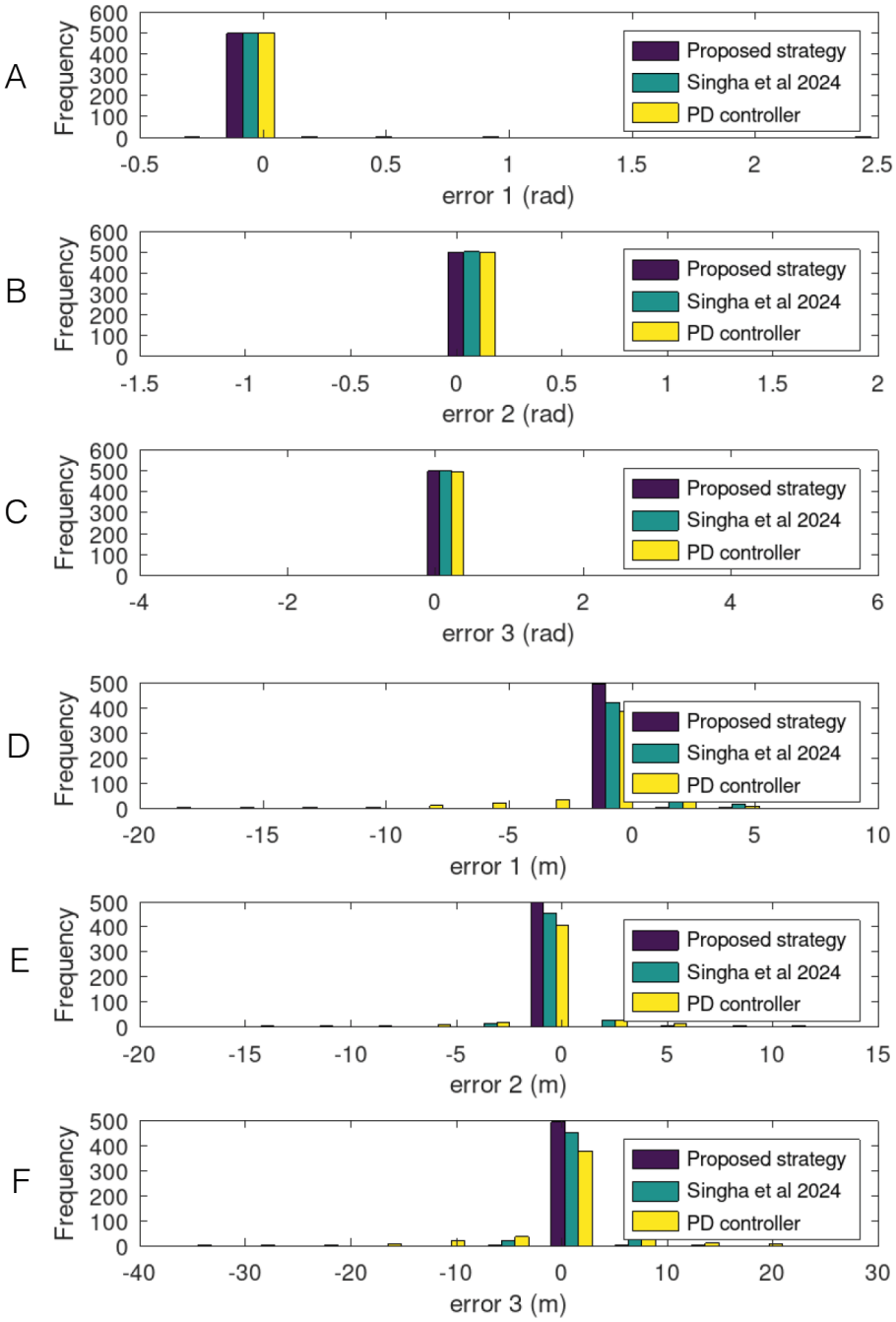

Figure 9. Histogram for the angular and position (A–C) Angular variables. (D–F) Position variables Abbreviations: PD: Proportional derivative; UAV: Unmanned aerial vehicle.

Finally, Figures 7 and 8 show the rotor torques along with the constrained inputs with the calculation of $A(q)\lambda$. It was verified how these variables evolve in time, proving that the torque of the quadrotor unmanned aerial vehicle is sufficiently small considering the constraints in this nonlinear dynamic system in the form of a port-Hamiltonian formulation.

Table 1, presents the RMSE obtained using the adapted control strategy in Singha et al.[47], the PD control strategy, and the proposed control strategy of this study. It can be observed that, in general, the RMSE yielded by the proposed control strategy was smaller than that of the strategy by Singha et al.[47] and the standard PD controller, which was expected, considering the design and mathematical representation of the quadrotor unmanned aerial vehicle. Tables 2 and 3 depict the respective mean and variance of the attitude and position errors. It was verified that the mean and variance are smaller for the proposed strategy compared to Singha et al.[47] and the PD controller. Apart from this, the histograms of the position and attitude errors are evinced in Figure 9, demonstrating the distribution of the errors for the proposed control strategy, the strategy by Singha et al.[47], and the PD controller, ratifying the results evinced in Table 2 and 3.

The RMSE formula used in Experiment 1 and 2 is given by:

$$RMSE = \sqrt{\frac{1}{N}\sum_{i=1}^{N}\|e_i\|^2} \tag{42}$$

In which N is the maximum number of samples of the error variable e_i.

5.2. Experiment 2

In this section, the results of the numerical simulation of the proposed control strategy in comparison with the strategies by Singha et al.[47] with the trajectory vector $q_d = [10\sin(t), 10\cos(t), 2t]^T$ m and a PD controller for the quadrotor unmanned aerial vehicle with non-holonomic constraints are reported. The difference between this numerical experiment and the previous one is that it involves a smooth, non-aggressive maneuver and a more realistic simulation scenario. The trajectory path shown in this research study consisted of a spiral, which was used as the reference trajectory in the position loop while generating the attitude reference to achieve the desired position.

5.2.1. Numerical Simulation of the Position Loop

As explained in the theoretical sections of this research study, the non-holonomic constraints was only considered in the attitude loop. The numerical simulation performed in this section demonstrates how, under a spiral trajectory, the complex variable neural network controller effectively tracks the desired trajectory of the quadrotor unmanned aerial vehicle. It is important to note that the position loop CVNN controller implements a decoupled control system approach. The results presented in this subsection include:

Figure 10 shows the trajectories in the x, y, and z axes. The results confirm that the proposed controller for the position loop provided superior performance compared to the strategies by Singha et al.[47] and PD control strategy. This improved performance is attributed to the flexibility and enhanced characteristics of the complex variable neural network controller in the position loop.

i Plots of the positions in each axis.
ii 3D plot of the trajectory tracking problem.
iii Plots of the control inputs in the position loop.

To corroborate the results shown in Figures 10, and 11 validates that the proposed control strategy achieved the lowest accumulated error compared to the approaches by Singha et al.[47] and the standard PD controller. Later in this section, Table 6 presents the RMSEs for both the attitude and position loops.

Figure 13 shows the 3D trajectory of the quadrotor unmanned aerial vehicle, further confirming the results presented in Figures 10, and 11. The figure demonstrates how the unmanned aerial vehicle accurately tracks the desired trajectory using the proposed control strategy. The complex variable neural network controller clearly outperformed other control approaches such those by Singha et al.[47] and the standard PD controller.

Figure 12 illustrates the control efforts generated by the proposed control strategy compared to those by Singha et al.[47] and the standard PD controller. The proposed approach showed optimal results with significantly smaller control effort compared to the other approaches, demonstrating greater efficiency.

5.2.2. *Numerical Simulation of the Attitude Loop*

For the attitude loop, non-holonomic constraints were considered. The non-holonomic force yielded

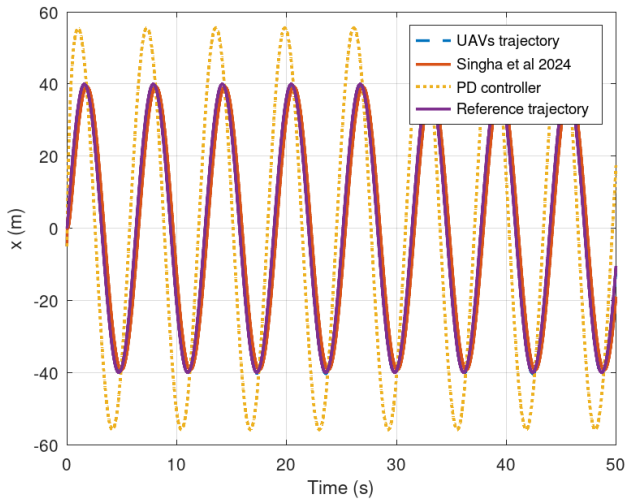

A

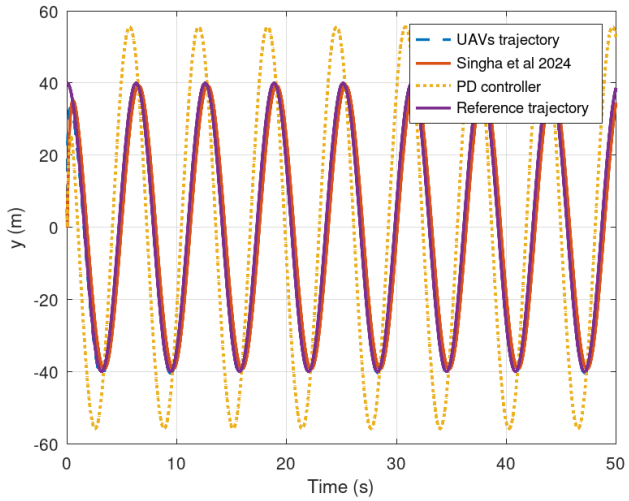

B

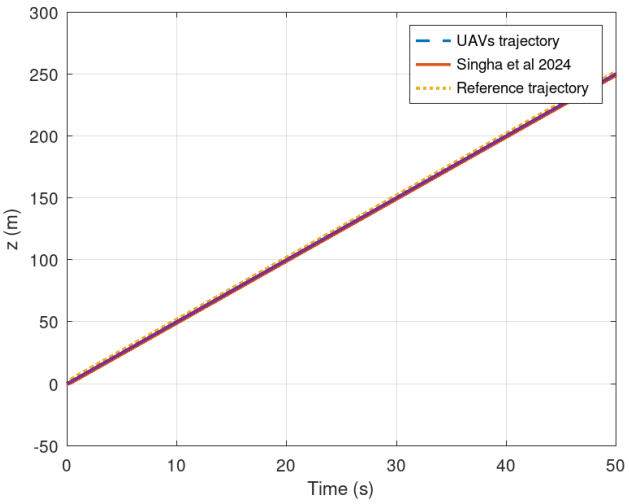

C

Figure 10. Position trajectory in the (A)x, (B)y and (C)z axis for experiment 2

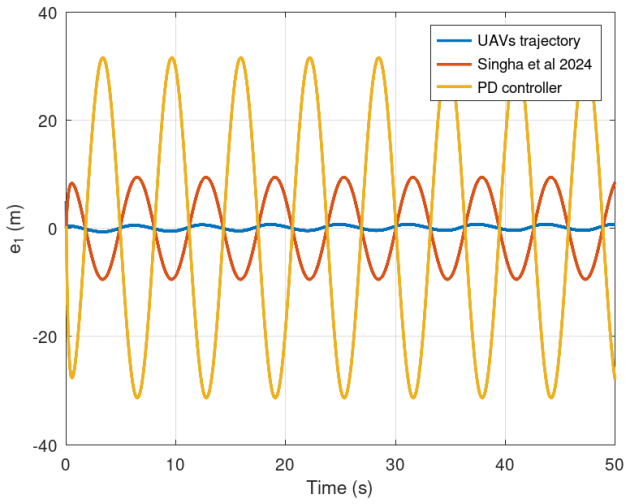

A

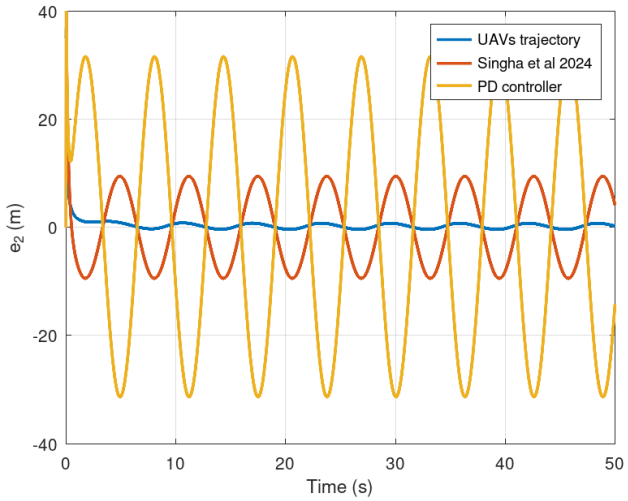

B

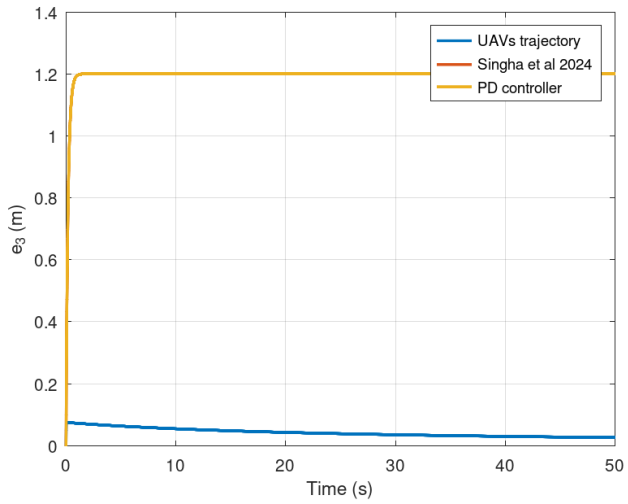

C

Figure 11. Position error in the (A)x, (B)y, and (C)z axes for experiment 2
Abbreviations: PD: Proportional derivative; UAV: Unmanned aerial vehicle.

Table 4. Qualitative comparative analysis of the different strategies for the position loop

Control approach	**Advantages**	**Disadvantages**
Proposed control strategy	The root mean square error is reduced with a small number of neurons or nodes.	If more nodes are needed, a higher computational effort is needed.
(Singha et al. 2024) [47]	It is a simple and fast control strategy for hardware implementation.	The performance is difficult to obtain due to uncertainties and disturbances.
Standard proportional derivative controller	Extremely simple.	If the gains of the proportional derivative controller are too high, then the closed loop performance is degraded.

Table 5. Qualitative comparative analysis of different strategies the attitude loop

Control approach	**Advantages**	**Disadvantages**
Proposed control strategy	The root mean square error is reduced with a small number of neuron or nodes. Additionally, Non-holonomic behavior is estimated better.	Computational complexity is high.
(Singha et al. 2024)[47]	It is a simple and fast control strategy for hardware implementation.	Non-holonomic behavior is not well supported.
Standard proportional derivative controller	Extremely simple.	If the gains of the proportional derivative controller are too high, then the closed loop performance is degraded, specially when non-holonomics contraints are included in the attitude loop dynamics.

Table 6. Comparison of root mean square errors of different strategies for Experiment 2

Variables	Normalized values of the root mean square error
(Position) Proposed approach	1.4113 m
(Position)(Singha et al., 2024)[47]	9.6421 m
(Position) proportional derivative controller	31.482 m
(Attitude) Proposed approach	0.044716 rads
(Attitude) (Singha et al., 2024)[47]	0.042833 rads
(Attitude) proportional derivative controller	0.058856 rads

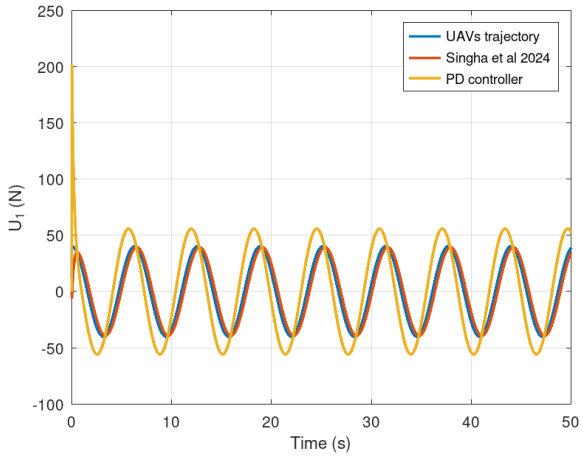

A

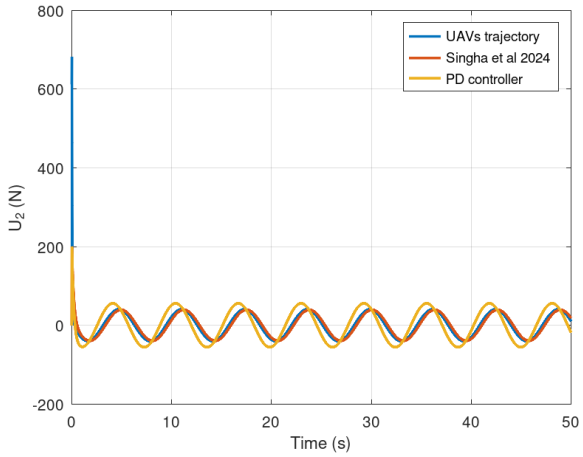

B

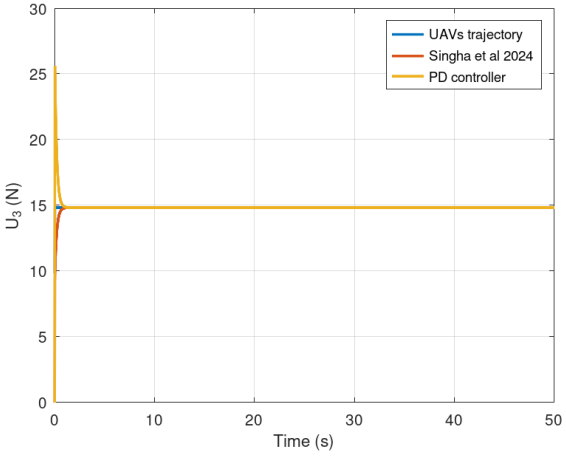

C

Figure 12. Input variables in the (A)x, (B)y, and (C)z axes for experiment 2
Abbreviations: PD: Proportional derivative; UAV: Unmanned aerial vehicle.

the force generated by the dynamic system constraints of the quadrotor unmanned aerial vehicle. These constraints were applied only to the attitude loop to ensure that the orientation of the quadrotor remains within an appropriate region. This subsection presents and discusses the plots of the attitude loop to examine the position dynamic loop performance.

The angular momentum trajectories in the x, y, and z axes are shown in Figure 14. The results show that the reference momentum was tracked more efficiently by the proposed control strategy

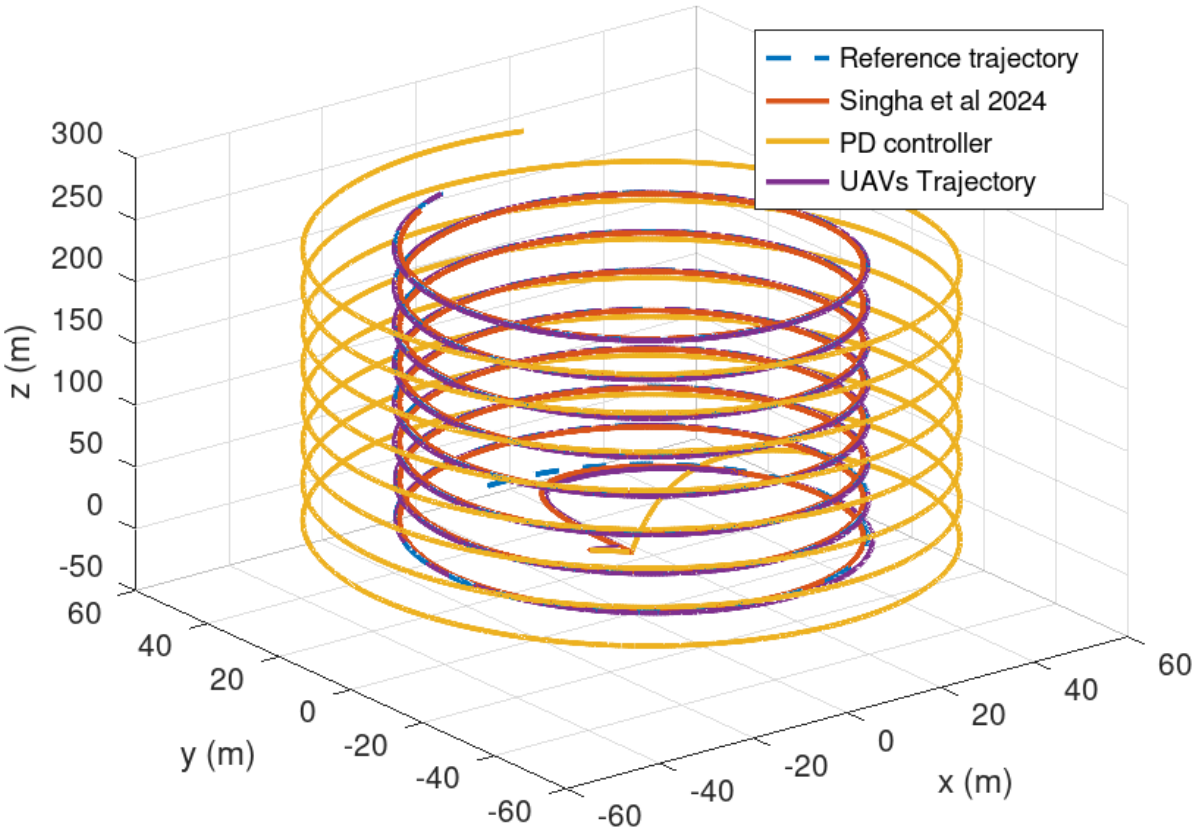

Figure 13. Three-dimensional trajectory of the quadrotor unmanned aerial vehicle
Abbreviations: PD: Proportional derivative; UAV: Unmanned aerial vehicle.

Table 7. Mean comparative table for different strategies for Experiment 1

Variables	Proposed approach	(Singha et al., 2024)[47]	Proportional derivative controller
x (m)	0.1126	-0.086144	0.3826
y (m)	0.3825	0.1338	0.3381
z (m)	0.042235	1.1957	-2.0287
a_1 (rad)	-2.5556×10^{-4}	-3.6875×10^{-4}	3.6391×10^{-4}
a_2 (rad)	5.8944×10^{-4}	6.9451×10^{-4}	1.0503×10^{-3}
a_3 (rad)	0.014782	0.014787	0.014851

Table 8. Variance comparative table for the performance of different strategies for Experiment 1

Variables	Proposed approach	(Singha et al., 2024)[47]	Proportional derivative controller
x (m)	0.1804	43.799	486.44
y (m)	1.6509	47.732	500.49
z (m)	1.7255×10^{-4}	2.5030×10^{-3}	0.010992
a_1 (rad)	7.9682×10^{-4}	7.6049×10^{-4}	1.6473×10^{-3}
a_2 (rad)	9.8406×10^{-4}	8.5512×10^{-4}	1.5954×10^{-3}
a_3 (rad)	4.3760×10^{-8}	9.9163×10^{-8}	2.9834×10^{-7}

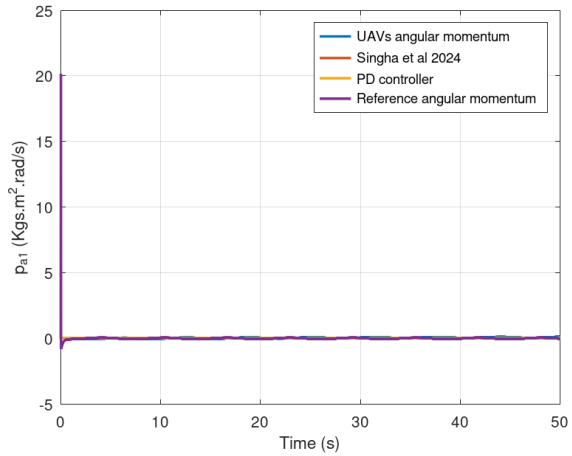

A

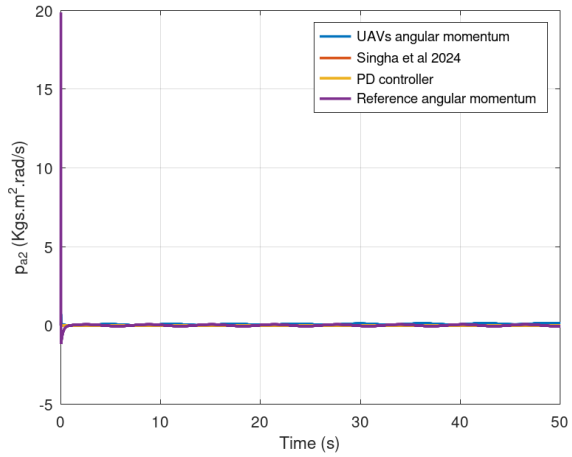

B

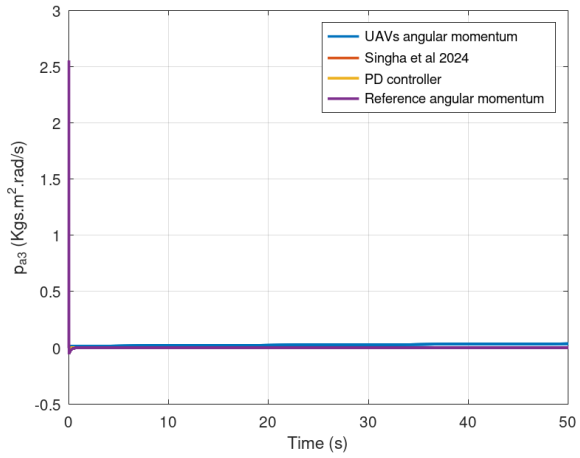

C

Figure 14. Angular momentum trajectory in the (A)x, (B)y, and (C)z axes for experiment 2
Abbreviations: PD: Proportional derivative; UAV: Unmanned aerial vehicle.

compared to the approach by Singha et al.[47] and the standard PD controller.

Figure 15 displays the error variables of the angular velocity. These error variables represent the difference between the desired angular velocity generated by the position loop and the actual angular velocity. Unlike other control strategies in the literature, our approach demonstrated that despite the presence of non-holonomic constraints in the attitude loop, the effectiveness of both the attitude and position loops ensured that the controller action

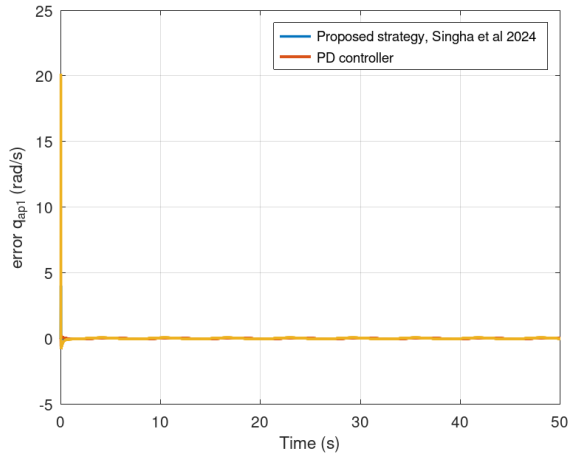

A

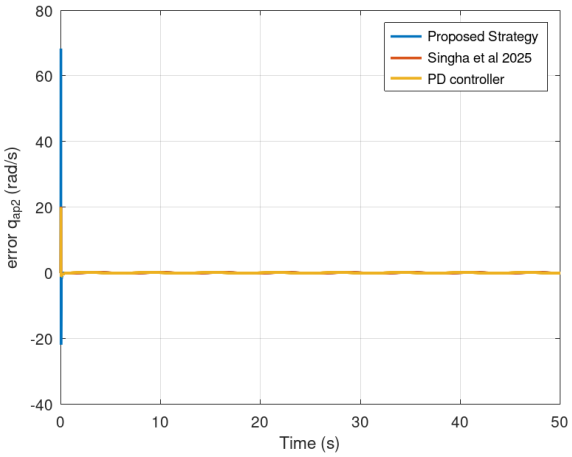

B

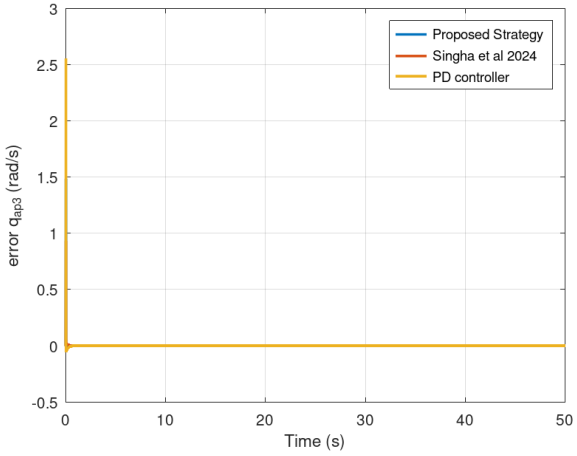

C

Figure 15. Error of the angular velocity in the (A)x, (B)y and (C)z axes for experiment 2 Abbreviations: PD: Proportional derivative; UAV: Unmanned aerial vehicle.

drives the state variables of the system in the port-Hamiltonian formulation to their desired values.

Figure 16 presents the torques generated by the four rotor propellers of the quadrotor unmanned aerial vehicle. The non-holonomic constraints helped maintain the rotor torques within appropriate operational ranges. These rotor torques are denoted as T_1, T_2, T_3 and T_4.

Figure 17 shows the torques generated by the non-holonomic constraints, where $A(q)\lambda$ was computed to achieve the desired value in

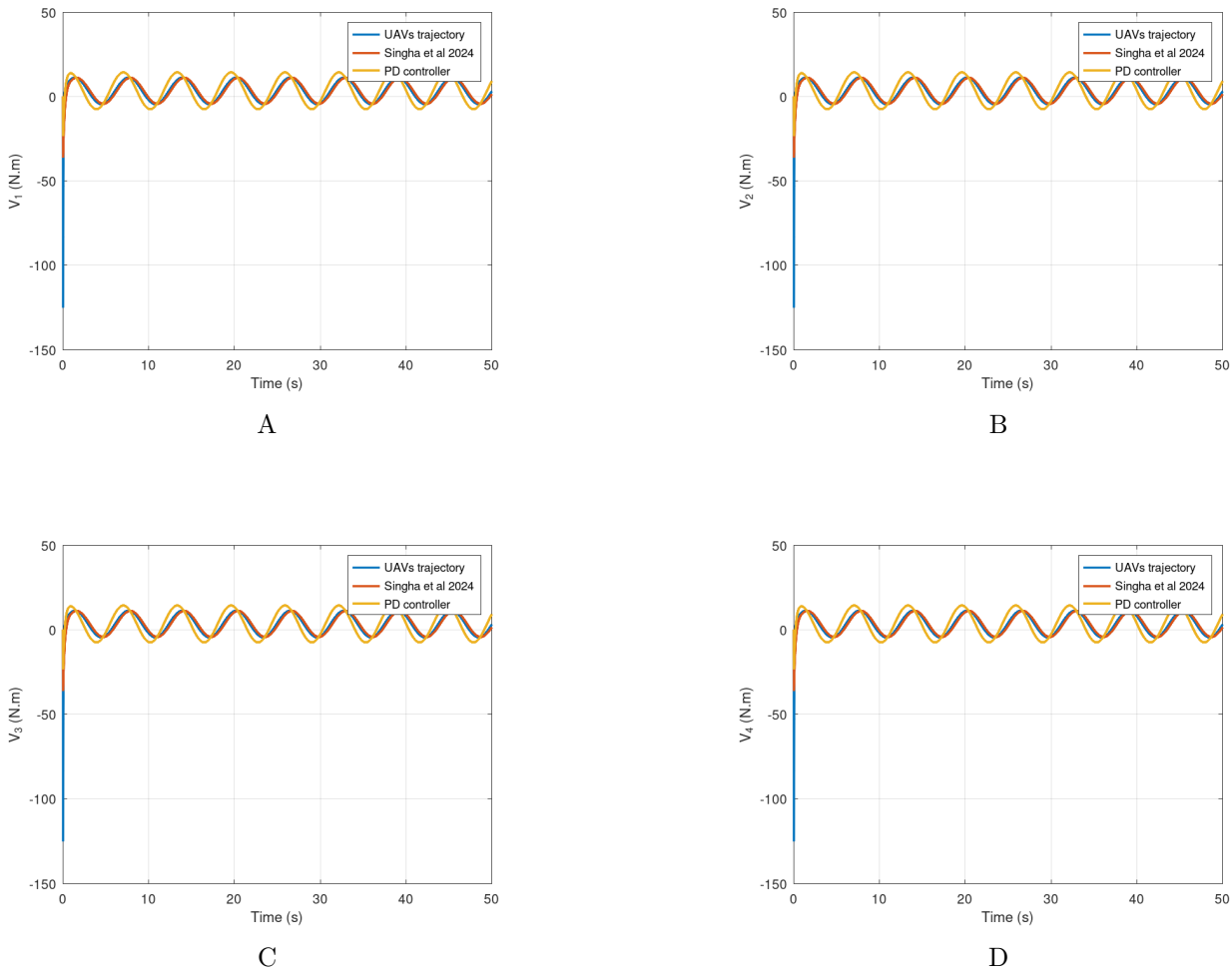

Figure 16. Torque of the four rotors of the quadrotor unmanned aerial Torque of rotor (A) 1, (B) 2, (C) 3, and (D) 4 vehicle for experiment 2
Abbreviations: PD: Proportional derivative; UAV: Unmanned aerial vehicle.

finite time. The figure demonstrates that the non-holonomic input is maintained near the origin at minimal values, so the constraints generated only the small effort required by the control action.

Table 5 presents a qualitative comparative analysis between the proposed control strategy, the approach by Singha et al.,[47] and the standard PD controller implemented in the attitude loop.

Table 6 presents the RMSE of the norm of the position q_x and attitude loop q_a. For the position loop, the proposed control approach achieved the lowest RMSE. For the attitude loop, the approach in[47] showed slightly better results, followed closely by our proposed strategy, with the PD controller showing the highest error. It is important to note that while the PD controller can be effective in certain scenarios, its performance significantly degrades with higher gains and in the presence of uncertainties and disturbances.

Table 7, and 8 show the position and attitude errors mean and variances, evincing in this second experiment, corroborating the results in Table 2, and 3 are corroborated. Figure 18 shows the histogram of the attitude and position errors. This corroborates that the results are extremely good for this numerical setup.

5.3. Computational Effort Analysis

The neural network implemented in this study is a complex-valued neural network. Its computational complexity is on the order of $\mathcal{O}(n^2)$, which is comparable to that of real-valued neural networks. This occurs because the complex variable neural network controller implemented in this research study is separated into the real and imaginary neural network controller components. The computational complexity indicates that if the complex variable neural network controller increases the number of nodes or neurons, the computational effort increases by n^2, taking into consideration that weight matrices are implemented in the neural network controller. As explained before, the

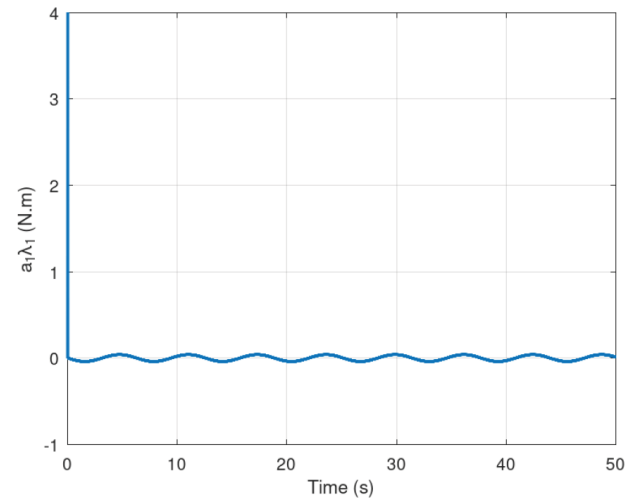

A

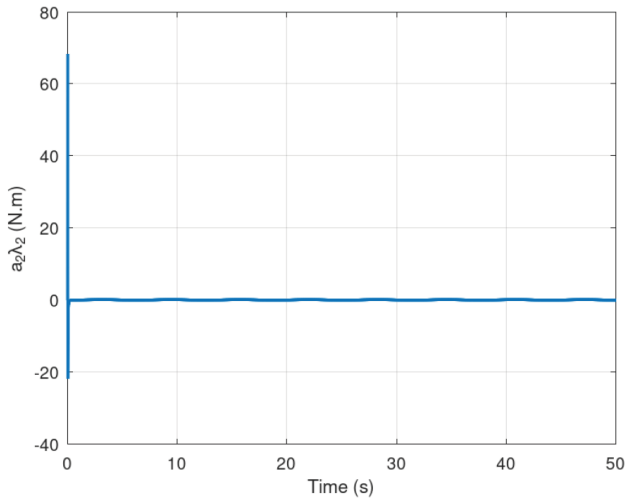

B

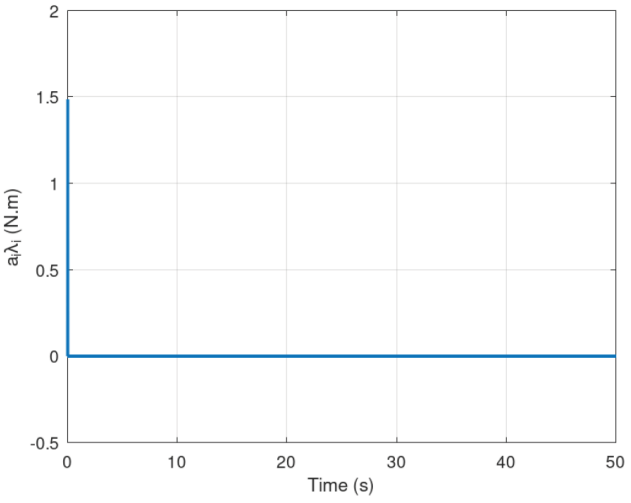

C

Figure 17. Constrained inputs with the calculation of $A(q)\lambda$, (A)x, (B)y, and (C)z axes for experiment 2 Abbreviations: PD: Proportional derivative; UAV: Unmanned aerial vehicle.

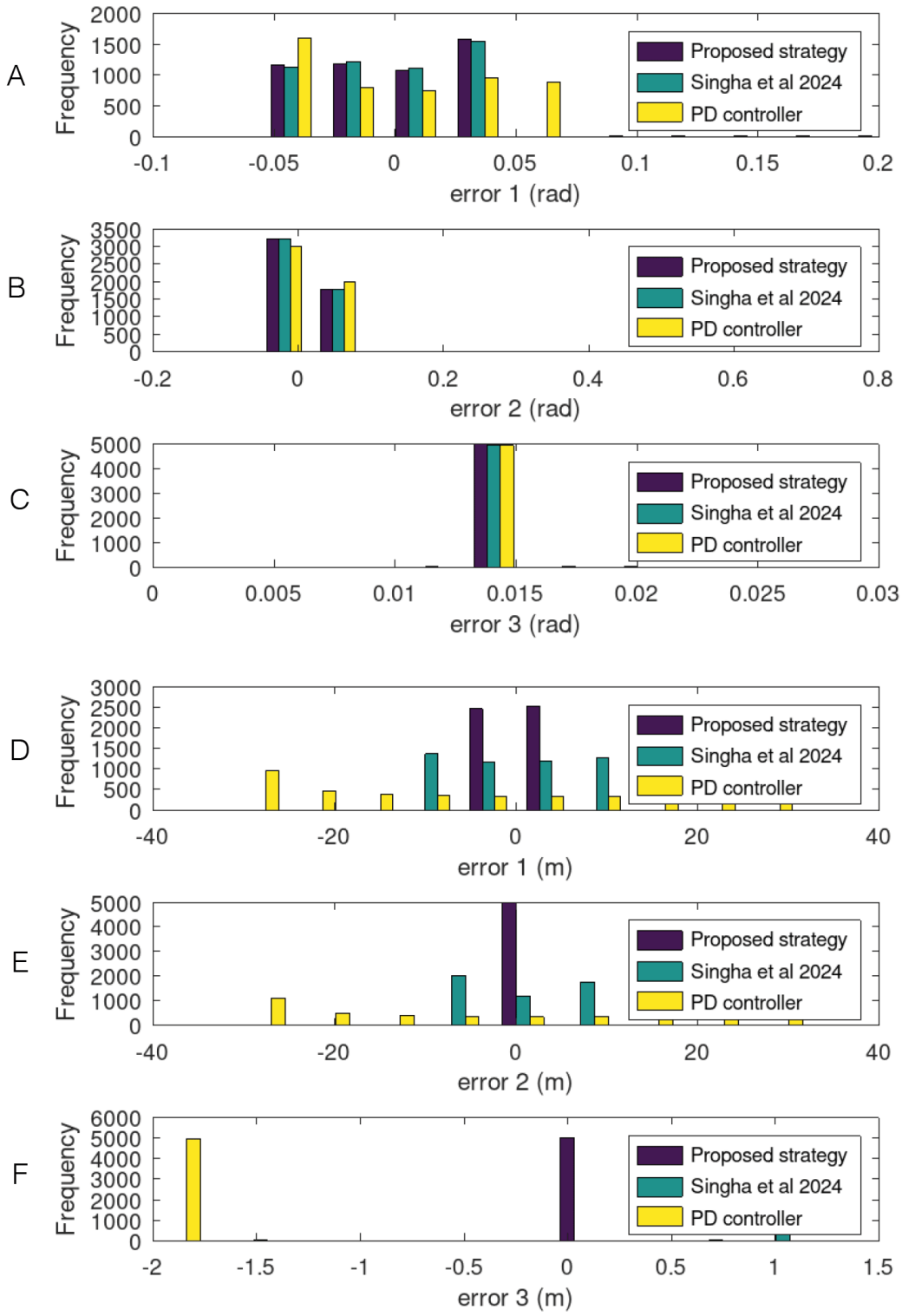

Figure 18. Histogram for the angular and position (A–C) Angular variables. (D–F) Position variables for experiment 2
Abbreviations: PD: Proportional derivative; UAV: Unmanned aerial vehicle.

computational effort is the same as a real-valued neural network or even as other types of neural networks, such as quaternion neural networks. Moreover, the advantage over real-valued neural networks is that the complex variable neural network possesses two degrees of freedom, making it more efficient compared with this type of neural network. The implementation of complex variable neural networks in hardware in the loop is very straightforward, considering that

the computational effort is crucial when neural networks are implemented as controllers in real-time experimental setups.

6. Discussion

According to the theoretical and experimental results of this research study, the trajectory position tracking of a quadrotor unmanned aerial vehicle was achieved satisfactorily. The numerical simulations confirm effective trajectory tracking for the unmanned aerial vehicle quadrotor along a spiral trajectory. A notable advantage of our approach is that the complex variable neural network controller performs effectively even with a small number of neurons and nodes. Due to the implementation of the Lyapunov function for control law synthesis, the CVNN controller weights do not require adjustment for nominal performance. Nevertheless, further performance optimization could be achieved through fine-tuning using algorithms such as particle swarm optimization. Despite using relatively simple parameter tuning, our results demonstrate that the position loop is controlled efficiently through the implemented CVNN controller structure and architecture.

We intentionally included non-holonomic constraints in the port-Hamiltonian formulation of the attitude loop dynamics. This design choice prevents forbidden orientations of the unmanned aerial vehicle during operation. For example, in the spiral trajectory tracking problem, the non-holonomic constraints ensured that the UAV does not make sudden, potentially destabilizing turns. This feature becomes particularly important in practical applications where the UAV might carry payloads or operate in environments where orientation constraints are critical for safety and performance. The ability to maintain appropriate orientation while following complex trajectories represents a significant improvement over traditional control approaches that do not explicitly account for such constraints within their formulation.

It is important to clarify that issues such as controllability and observability were not considered in this research study. Due to the high coupling between the position and attitude loops and nonlinearities found in the dynamic system, these issues are difficult to analyze. Other studies, such as Shukla et al.,[48,49] are available in which the controllability of a complex semilinear stochastic system is analyzed and the controllability of a second order complex system are evinced respectively. These references are important to mention, as the coupled or decoupled controllability analysis of the quadrotor dynamics must be taken into consideration. However, it is important to clarify that global closed loop stability of the errors variables for the position and attitude loops are ensured by the proposed neural network controller. The complex variable neural network controller ensures the convergence of the error variables to zero in finite time. Taking into consideration that CVNN are able to "learn" the appropriate control dynamics according to the position and attitude loops dynamics, this aspect ease the implementation of a "soft" controller for this complex system. Readers can refer to Rezapour et al.[50] for more details.

It is important to ratify that some dynamical system issues such as disturbances and parameter uncertainties are not considered in this research study. However, the proposed control strategy can be extended to a dynamic system with parametric uncertainties easily; in this way, the variation in parameters such as the quadrotor mass and its inertias can be considered. Disturbance rejection controllers can also be obtained, clarifying that, in this study, these issues were not considered but they will be considered as an extension to the results shown in this work.

7. Conclusion

This work has demonstrated the effectiveness of a CVNN controller for trajectory tracking in quadrotor UAV within the port-Hamiltonian framework. By decoupling the attitude and position control loops and implementing non-holonomic constraints exclusively in the attitude loop, we achieved robust control that maintains appropriate orientation constraints during trajectory tracking. The Lyapunov-based controller synthesis provided theoretical guarantees of stability while numerical experiments validated superior performance compared to existing approaches. Our CVNN controller exhibited significantly lower position tracking errors (RMSE of 1.4113 m compared to 9.6421 m for the benchmark method) while requiring minimal computational resources. The inclusion of non-holonomic constraints successfully prevented forbidden orientations of the UAV, particularly beneficial for applications involving payload transportation or requiring smooth trajectories. The control architecture demonstrated excellent performance with minimal tuning, though further optimization could be achieved through techniques such as particle swarm optimization. This research

provides a solid foundation for future work in advanced UAV control strategies that maintain structural properties while guaranteeing robust performance under operational constraints. The main results of this work is that the proposed control strategy provided the required control effort for the stabilization of the errors in the position and attitude loops of a quadrotor unmanned aerial vehicle. As explained before, as a future direction, the design of neural networks controllers accounting for uncertainties and disturbances will be considered.

Acknowledgments

This paper is derived from a research grant funded by the Research, Development, and Innovation Authority (RDIA) - Kingdom of Saudi Arabia, with grant number (13382-psu-2023-PSNU-R-3-1-EI-). The authors would like to thank Prince Sultan University, Riyadh, Saudi Arabia, for supporting the article processing charges (APC) of this publication. The authors especially acknowledge the Automated Systems and Computing Lab (ASCL) at Prince Sultan University, Riyadh, Saudi Arabia.

Funding

This study is supported by a research grant funded by the Research, Development, and Innovation Authority (RDIA) - Kingdom of Saudi Arabia, with grant number (13382-psu-2023-PSNU-R-3-1-EI-). The authors would like to thank Prince Sultan University, Riyadh, Saudi Arabia, for supporting the article processing charges (APC) of this publication.

Conflict of interest

The authors declare no conflict of interest.

Author contributions

Conceptualization: Fernando Serrano, Ahmad Taher Azar
Formal analysis: Fernando Serrano, Ahmad Taher Azar, Ahmed Redha Mahlous
Funding: Ahmed Redha Mahlous
Investigation: Fernando Serrano, Ahmad Taher Azar, Ahmed Redha Mahlous
Methodology: Fernando Serrano
Supervision: Ahmad Taher Azar, Saim Ahmed
Writing–original draft: Fernando Serrano
Writing–review & editing: Fernando Serrano, Saim Ahmed, Ahmad Taher Azar

Availability of data

Not applicable.

AI tools statement

All authors confirm that no AI tools were used in the preparation of this manuscript.

References

1. Pu J, Zhang Q, Zhao W, Zhang W, Qin Z, Zhang Y. Research on refined UAV inspection method of wind/solar power stations based on YOLOv8. *J Eng Appl Sci.* 2025;72(1). https://www.doi.org/10.1186/s44147-025-00576-1
2. Li X, Wang A. Forest pest monitoring and early warning using UAV remote sensing and computer vision techniques. *Sci Rep.* 2025;15(1). https://www.doi.org/10.1038/s41598-024-84464-3
3. Tarpenning MS, Bramante JT, Coombe KD, et al. Comparison of unmanned aerial vehicle imaging to ground truth walkthroughs for identifying and classifying trash sites serving as potential Aedes aegypti breeding grounds. *Parasit Vectors.* 2025;18(1). https://www.doi.org/10.1186/s13071-025-06706-1
4. Xu P, Sulaiman NAA, Ding Y, Zhao J. Innovative segmentation technique for aerial power lines via amplitude stretching transform. *Sci Rep.* 2025;15(1). https://www.doi.org/10.1038/s41598-025-86753-x
5. Van Haeften S, Smith D, Robinson H, et al. Unmanned aerial vehicle phenotyping of agro-nomic and physiological traits in mungbean. *Plant Phenome J.* 2025;8(1). https://www.doi.org/10.1002/ppj2.70016
6. Li J, Ling M, Fu B, et al. UAV based smart grazing: a prototype of space-air-ground integrated grazing IoT networks in Qinghai-Tibet plateau. *Discov IoT.* 2025;5(1). https://www.doi.org/10.1007/s43926-025-00114-8
7. Liller J, Goel R, Aziz A, Hester J, Nguyen P. Development of a battery free, solar powered, and energy aware fixed wing unmanned aerial vehicle. *Sci Rep.* 2025;15(1). https://www.doi.org/10.1038/s41598-025-90729-2
8. Han G. Bio-inspired swarm intelligence for en-hanced real-time aerial tracking: integrating whale optimization and grey wolf optimizer algo-rithms. *Discov Artif Intell.* 2025;5(1). https://www.doi.org/10.1007/s44163-025-00237-5
9. Liu Y, Zhang H, Zheng H, Li Q, Tian Q. A spherical vector-based adaptive evolutionary particle swarm optimization for UAV path planning under threat conditions. *Sci Rep.* 2025;15(1). https://www.doi.org/10.1038/s41598-025-85912-4
10. Bouzid Y, Siguerdidjane H, Bestaoui Y, Zareb M. Energy Based 3D Autopilot for VTOL UAV Un-der Guidance and Navigation Constraints. *J Intell Robot Syst Theory Appl.*

2017;87(2):341–362.
https://www.doi.org/10.1007/s10846-016-0441-1
11. Rashad R, Engelen JBC, Stramigioli S. Energy Tank-Based Wrench/Impedance Control of a Fully-Actuated Hexarotor: A Geometric Port-Hamiltonian Approach. In: 2019 International Conference on Robotics and Automation (ICRA). *IEEE*; 2019:6418-6424.
https://www.doi.org/10.1109/icra.2019.8793939
12. Souza C, Raffo GV, Castelan EB. Passivity Based Control of a Quadrotor UAV. *IFAC-PapersOnLine*. 2014;47(3):3196-3201.
https://www.doi.org/10.3182/20140824-6-za-1003.02335
13. Rashad R, Califano F, Stramigioli S. Port-Hamiltonian Passivity-Based Control on SE(3) of a Fully Actuated UAV for Aerial Physical Interaction Near-Hovering. *IEEE Robotics and Automation Letters*. 2019;4(4):4378–4385.
https://www.doi.org/10.1109/LRA.2019.2932864
14. Avazzadeh Z, Hassani H, Eshkaftaki AB, Ebadi M, Agarwal P. Optimal solution of nonlinear 2D variable-order fractional optimal control problems using generalized Bessel polynomials. *J Vib Control*. 2025;31(7-8):1457-1471.
https://doi.org/10.1177/10775463241227475
15. Zhou W, Xu Z, Wu Y, Xiang J, Li Y. Energy-based trajectory tracking control of under-actuated unmanned surface vessels. *Ocean Eng*. 2023;288.
https://www.doi.org/10.1016/j.oceaneng.2023.116166
16. Ma L, Pang S, He Y, Wu Y, Li Y, Zhou W. Passivity-Based Sliding Mode Control for the Ro-bust Trajectory Tracking of Unmanned Surface Vessels Under External Disturbances and Model Uncertainty. *J Mar Sci Eng*. 2025;13(2).
10.3390/jmse13020364
17. Lv C, Chen J, Yu H, Chi J, Yang Z. Adaptive NN state error PCH trajectory tracking control for unmanned surface vessel with uncertain-ties and input saturation. *Asian J Control*. 2023;25(5):3903–3919.
https://www.doi.org/10.1002/asjc.3076
18. Jin L, Yu S, Zhao Q, Shi G, Wu X. Fixed-time H-infinity tracking control of unmanned underwater vehicles with disturbance rejection via Port-Hamiltonian framework. *Ocean Eng*. 2024;293.
https://www.doi.org/10.1016/j.oceaneng.2023.116533
19. Wang Z, Zhang Y, Gao Q, Chen J, Lv C. Fourier-Based Formation Control of Multiple Unmanned Surface Vessels Using a State Error Port Control Hamiltonian Framework. In: 2024 China Automation Congress (CAC). *IEEE*; 2024:2490-2495.
https://www.doi.org/10.1109/cac63892.2024.10865534
20. Lv C, Wang Z, Zhang Y, Chen J, Yu H. Cooperative formation control of multiple unmanned surface vessels based on state error port control Hamiltonian framework. *Ocean Eng*. 2024;313.
https://www.doi.org/10.1016/j.oceaneng.2024.119410
21. Feng L, Yu J, Hu C, Yang C, Jiang H. Nonseparation Method-Based Finite/Fixed-Time Synchronization of Fully Complex-Valued Discontinuous Neural Networks. *EEE Trans Cybern*. 2021;51(6):3212–3223.
https://www.doi.org/10.1109/TCYB.2020.2980684
22. Jayanthi N, Santhakumari R. Passivity analysis of multiple time-varying time delayed complex vari-able neural networks in finite-time. *Math Model Comput*. 2021;8(4):842–854.
https://www.doi.org/10.23939/mmc2021.04.842
23. Liu B, Mei X, Jiang H, Wu L. A Nonpenalty Neurodynamic Model for Complex-Variable Optimization. *Discrete Dyn Nat Soc*. 2021;2021.
https://www.doi.org/10.1155/2021/6632257
24. Sriraman R, Manoj N, Agarwal P, Vigo-Aguiar J, Jain S. Event-triggered control for exponential synchronization of reaction–diffusion fractional-order Clifford-valued delayed neural networks and its application to image encryption. *Neurocomputing*. 2025;648:130604.
https://doi.org/10.1016/j.neucom.2025.130604
25. Chen W, Ding Y, Weng F, Liang C, Li J. Global Fast Terminal Fuzzy Sliding Mode Control of Quadrotor UAV Based on RBF Neural Network. *Sensors*. 2025;25(4).
https://www.doi.org/10.3390/s25041060
26. Xiong JJ, Li C. Neuroadaptive Sliding Mode Tracking Control for an Uncertain TQUAV With Unknown Controllers. *Int J Robust Nonlin*. 2025;35(2):579–590.
https://www.doi.org/10.1002/rnc.7664
27. Li J, Wu L. A multiple connected recurrent neural network based super-twisting terminal sliding mode control for quad-rotor UAV. *Eur J Control*. 2025;83.
https://www.doi.org/10.1016/j.ejcon.2025.101220
28. Chai Y, Yang Z, Yu H, Liang X, Han J. Adaptive Trajectory Tracking Control for Double-Pendulum Aerial Transportation System. *IEEE Trans Ind Electron*. 2025.
https://www.doi.org/10.1109/TIE.2025.3536563
29. Mahmood A, Rehman uF, Okasha M, Saeed A. Neural Adaptive Sliding Mode Control for Camera Positioner Quadrotor UAV. *Int J Aeronaut Space Sci*. 2025;26(2):733–747.
https://www.doi.org/10.1007/s42405-024-00781-x
30. Li B, Chen M, Qi S, Peng K. Finite-time fault-tolerant control of attitude control system of quadrotor UAV based on neural network disturbance observer. *Neural Comput Appl*. 2025;37(7):5597–5606.
https://www.doi.org/10.1007/s00521-024-10927-3

31. Wu LF, Wang Z, Rastgaar M, Mahmoudian N. Adaptive velocity control for UAV boat landing: A neural network and particle swarm optimization approach. *J Intell Robot Syst.* 2025;111(1). https://www.doi.org/10.1007/s10846-024-02201-4
32. Peng C, Qiao G, Ge B. Dynamic Cascade Spiking Neural Network Supervisory Controller for a Non-planar Twelve-Rotor UAV. *Sensors.* 2025;25(4). 10.3390/s25041177
33. Zhang Y, Sha H, Peng R, et al. Adaptive Observer-Based Neural Network Control for Multi-UAV Systems with Predefined-Time Stability. *Drones.* 2025;9(3). https://www.doi.org/10.3390/drones9030222
34. Bekhiti A, Souanef T, Toubakh H, Horri N, Kafi MR, Bouzid Z. Adaptive UAV Control with Sensor and Actuator Faults Recovery. *Aerospace.* 2025;12(3). https://www.doi.org/10.3390/aerospace12030261
35. van der Schaft A, Maschke B. Differential operator Dirac structures. *IFAC-PapersOnLine.* 2021;54(19):198-203. https://doi.org/10.1016/j.ifacol.2021.11.078
36. Ye Y, Li Z, Li C, Shen S, Ma WX. A generalized Dirac soliton hierarchy and its bi-Hamiltonian structure. *Appl Math Lett.* 2016;60:67-72. https://doi.org/10.1016/j.aml.2016.04.010
37. Yoshimura H, Gay-Balmaz F. Dirac structures in nonequilibrium thermodynamics. *IFAC-PapersOnline.* 2018;51(3):31-37. https://www.doi.org/10.1016/j.ifacol.2018.06.009
38. Kumar N, Zwart H, van der Vegt J. Dirac structure for linear dynamical systems on Sobolev spaces. *J Math Anal Appl.* 2025;549(2):129493. https://doi.org/10.1016/j.jmaa.2025.129493
39. Gay-Balmaz F, Yoshimura H. Variational and Dirac structures for interconnected distributed-discrete systems. *IFAC-PapersOnline.* 2024;58(6):286-291. https://doi.org/10.1016/j.ifacol.2024.08.295
40. Tortorella AG. The deformation L-infinity algebra of a Dirac–Jacobi structure. *Differential Geometry and its Applications.* 2022;80:101846. https://doi.org/10.1016/j.difgeo.2021.101846
41. Seslija M, van der Schaft A, Scherpen JMA. Reduction of Stokes-Dirac structures and gauge symmetry in port-Hamiltonian systems. *IFAC-PapersOnLine.* 2012;45(19):114-119. https://www.doi.org/10.3182/20120829-3-it-4022.00030
42. Lamoline F, Hastir A. On Dirac structure of infinite-dimensional stochastic port-Hamiltonian systems. *Eur J Control.* 2024; 75:100924. https://doi.org/10.1016/j.ejcon.2023.100924
43. Cervera J, van der Schaft A, Ban˜os A. Interconnection of port-Hamiltonian sys-tems and composition of Dirac structures. *Automatica* 2007;43(2):212-225. https://doi.org/10.1016/j.automatica.2006.08.014
44. Azar AT, Serrano FE, Koubaa A, Taha MA, Kamal NA. Fast terminal sliding mode controller for high speed and complex maneuvering of unmanned aerial vehicles. In: Unmanned Aerial Systems. Elsevier; 2021:203-230. https://www.doi.org/10.1016/b978-0-12-820276-0.00016-9
45. Fujimoto K, Sakai S, Sugie T. Passivity Hamiltonian based control of a class of systems with non-holonomic Automatica. 2012;48(12):constraints. 3054-3063. https://doi.org/10.1016/j.automatica.2012.08.032
46. Hui M, Zhang J, Iu HHC, Yao R, Bai L. A novel intermittent sliding mode con-trol approach to finite-time synchroniza-tion of complex-valued neural networks. *Neurocomputing.* 2022;513: 181-193. https://doi.org/10.1016/j.neucom.2022.09.111
47. Singha A, Thakur S, Ray AK. Lyapunov based trajectory tracking controller for a quadro-tor UAV with nonholonomic constraints. e-Prime - Advances in Electrical Engineering, Electronics and Energy. 2024;8:100617. https://doi.org/10.1016/j.prime.2024.100617
48. Shukla A, Arora U, Sukavanam N. Approximate controllability of retarded semilinear stochastic system with non local conditions. *Appl Math Comput.* 2015;49:513–527. https://doi.org/10.1007/s12190-140851-9
49. Shukla A, Sukavanam N. Interior approximate controllability of second-order semi-linear control systems. *Int J Control.* 2024;97(3):615–624. https://www.doi.org/10.1080/00207179.2022.2161013
50. Rezapour S, Henr´ıquez HR, Vijayakumar V, Nisar KS, Shukla A. A Note on Existence of Mild Solutions for Second-Order Neutral Integro-Differential Evolution Equations with State-Dependent Delay. *Fractal Fract.* 2021;5(3). https://www.doi.org/10.3390/fractalfract5030126

Fernando Serrano *received his BEng from the Central American Technical University (UNITEC) in Tegucigalpa, Honduras in 2003 and M. Sc. in Electrical Engineering from Florida International University in Miami, FL, USA in 2007. He is an author of some publications and presentations in journals, book chapters and conference and he is actually collaborating with professors from Egypt, Spain, Honduras, El Salvador, Saudi Arabia and Mexico. Besides, he is Ph.D. candidate of the automatic control Ph. D. program at Technical University of Catalonia in Barcelona, Spain. His research area are the control of complex systems, specifically and adaptive control.*

https://orcid.org/0000-0002-8800-7578

Saim Ahmed *received the B.Sc. degree in electronics from the Sir Syed University of*

Science and Technology, Pakistan, in 2009, the M.E. degree in industrial control and automation from Hamdard University, Pakistan, in 2013, and the Ph.D. degree in control science and engineering from Nanjing University of Science and Technology, China, in 2019. He is currently a Postdoctoral Researcher with the Automated Systems and Computing Lab (ASCL) in the Department of Computer Science, Prince Sultan University, Riyadh, Saudi Arabia. His research interests include the theory and applications of adaptive control, sliding mode control, time delay control, robotic manipulators, and nonlinearities and their compensation.
https://orcid.org/0000-0002-2302-705X

Ahmad Taher Azar *(Senior Member, IEEE) is a full Professor at College of Computer and Information Sciences (CCIS), Prince Sultan University, Riyadh, Saudi Arabia. He is a leader of Automated Systems and Computing Lab (ASCL), Prince Sultan University, Saudi Arabia. He is currently an editor for IEEE Transactions on Fuzzy Systems, IEEE Transactions on Neural Networks and Learning Systems, Springer's Human-centric Computing and Information Sciences, and Elsevier's Engineering Applications of Artificial Intelligence. Prof. Azar was named one of the top 2% of scientists in the world in Artificial Intelligence by Stanford University, based on single-year impact and career-long impact. These rankings were published by Stanford University in the PLOS journal and were based on the SCOPUS database. Prof. Azar has expertise in Artificial Intelligence, Control Theory and Applications, Robotics, Machine Learning, Computational Intelligence and dynamical system modeling. He has authored/co-authored over 600 research papers in prestigious peer-reviewed journals, book chapters, and conference proceedings.*
https://orcid.org/0000-0002-7869-6373

Ahmed Redha Mahlous *is an Associate Professor in the Department of Computer Science at Prince Sultan University (KSA). He earned a master's degree (MSc) from South Bank University (London, UK) and a PhD degree from the University of Bradford (UK). He worked as an IT consultant for a number of UK-based companies, and worked for several years as an academic instructor and as a Pearson VUE Exam Center Director at the Regional Cisco Academy (KSA). He holds multiple commercial certifications from Microsoft, Cisco, and Palo Alto, among others. His research interests include Cybersecurity, Networking, QoS, and Data mining. He is a reviewer for some prominent journals and has multiple scientific publications.*
https://orcid.org/0000-0001-7745-3428

An International Journal of Optimization and Control: Theories & Applications
(https://accscience.com/journal/ijocta)